REPORT DOCUMENTATION PAGE

1a. REPORT SECURITY CLASSIFICATION UNCLASSIFIED	1b. RESTRICTIVE MARKINGS
2a. SECURITY CLASSIFICATION AUTHORITY	3. DISTRIBUTION/AVAILABILITY OF REPORT Approved for public release; distribution unlimited
2b. DECLASSIFICATION/DOWNGRADING SCHEDULE	
4. PERFORMING ORGANIZATION REPORT NUMBER(S) TD 7913	5. MONITORING ORGANIZATION REPORT NUMBER(S)
6a. NAME OF PERFORMING ORGANIZATION Naval Underwater Systems Center 6b. OFFICE SYMBOL (If applicable)	7a. NAME OF MONITORING ORGANIZATION
6c. ADDRESS (City, State, and ZIP Code) New London Laboratory New London, CT 06320	7b. ADDRESS (City, State, and ZIP Code)
8a. NAME OF FUNDING/SPONSORING ORGANIZATION Naval Oceanographic Research & Devel. Activity 8b. OFFICE SYMBOL (If applicable) Code 113	9. PROCUREMENT INSTRUMENT IDENTIFICATION NUMBER
8c. ADDRESS (City, State, and ZIP Code)	10. SOURCE OF FUNDING NUMBERS PROGRAM ELEMENT NO. 62435N; PROJECT NO. A67001; TASK NO.; WORK UNIT ACCESSION NO.

11. TITLE (Include Security Classification) ACOUSTIC SCATTERING FROM COMPOSITE WIND-WAVE SURFACES III: FORWARD SCATTER INTENSITIES AND SPATIAL COHERENCE AT LOW AND HIGH FREQUENCIES AND SMALL GRAZING ANGLES FOR "BUBBLE-FREE" RÉGIMES

12. PERSONAL AUTHOR(S) David Middleton

13a. TYPE OF REPORT	13b. TIME COVERED	14. DATE OF REPORT (Year, Month, Day)	15. PAGE COUNT
	FROM 10/85 TO 12/86	1987, January 23	59

16. SUPPLEMENTARY NOTATION

17 COSATI CODES			18. SUBJECT TERMS (Continue on reverse if necessary and identify by block number)
FIELD	GROUP	SUB-GROUP	High Frequency, Low Frequency Scattering; Wind-Wave Surfaces, Forward Scatter, Spatial Coherence, Oblique and Snell Scattering.

19. ABSTRACT (Continue on reverse if necessary and identify by block number)

The present investigation continues the earlier studies of the author embodied in NUSC Technical Document TD-7025 [1] and Technical Report TR-7635 [2]. Underwater acoustic scattering from the random moving wind-wave surface of the ocean is again considered. Specifically, one is now concerned with both "high" O(5-20 kHz) and "low" O(0.2-2.0 kHz) frequency emissions and small grazing angles O(≤25°) with near-surface volume régimes which are effectively "bubble-free" [1] [2] for moderate to comparatively high mean wind states $\bar{U}_\infty$ = O(8-15 m/sec).

Cont'd

20 DISTRIBUTION/AVAILABILITY OF ABSTRACT ☐ UNCLASSIFIED/UNLIMITED ☒ SAME AS RPT ☐ DTIC USERS	21. ABSTRACT SECURITY CLASSIFICATION UNCLASSIFIED
22a NAME OF RESPONSIBLE INDIVIDUAL John Chester	22b. TELEPHONE (Include Area Code) (203) 440-4514 22c. OFFICE SYMBOL 3331

19. ABSTRACT (Continued)

The following are obtained here: analytic results at small grazing angles for: (I) coherent and incoherent forward scatter cross-sections at both high and low frequencies; (II) the coherent and incoherent spatial covariance functions of forward and obliquely scattered sound, likewise at high and low frequencies. In addition to the usual (linear) gravity-capillary wave surface components, the recently postulated soliton-surface layer, generated by nonlinear wind-wave interactions, is included [2] to account for the incoherent high-frequency effects observed experimentally [3]-[8].

Oblique and forward (Snell-angle) scattering is examined and discussed for both scattering cross-sections and surface coherence functions (SCF's). The latter provide a measure of the extent of spatial coherence obtaining at any given instant, on the average, between observation of the surface scattered acoustic field at any two points in the medium. Analytic results and numerical examples illustrate the general approach. Particular attention is given to forward scatter at the Snell angles.

NUSC Technical Document 7913
23 January 1987

0142

Acoustic Scattering From Composite Wind-Wave Surfaces III: Forward Scatter Intensities and Spatial Coherence at Low and High Frequencies and Small Grazing Angles for "Bubble-Free" Regimes

David Middleton
Office of the
Associate Technical Director
for Reseach and Technology

Naval Underwater Systems Center
Newport, Rhode Island / New London, Connecticut

PREFACE

This document is a continuation of work initiated under NUSC Project No. A67001, "High Frequency Acoustic Program." The present Principal Investigator of this project is J. B. Chester (Code 3331). The sponsoring activity is Naval Oceanographic Research and Development Activity (NORDA), Dr. R. Farwell (Code 243), Program Manager. Funding was provided under Program Element No. 62759. This document was prepared for J. B. Chester (Code 3331) by David Middleton, 127 E. 91 St., New York, NY 10128, under Contract No. N66604–85–M–C456 and in part under Contract Nos. N00140–84–M–MS42 and N00140–84–M–NM82.

The technical reviewers for this document were Dr. R. L. Deavenport (Code 3332) and J. B. Chester (Code 3331).

The author wishes to thank Dr. W. I. Roderick for his interest in this research. The author also would like to thank Dr. R. L. Deavenport and J. B. Chester for their suggestions and comments regarding the author's scatter model and results.

REVIEWED AND APPROVED: 23 January 1987

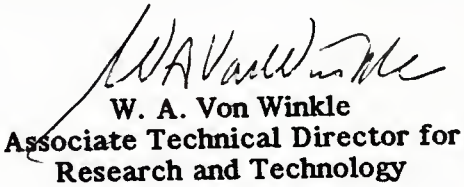

W. A. Von Winkle
Associate Technical Director for
Research and Technology

TABLE OF CONTENTS

LIST OF FIGURES

LIST OF PRINCIPAL SYMBOLS

A_o	signal amplitude
A_α	angle function
A, A_T	beam-pattern parameter
A_{REF}, A_1	beam-projected surface areas
$\mathcal{Q}_{T,\,R}$	beam patterns
$\hat{\alpha}_1$, $\hat{\alpha}_o$	wave direction angles
$2\underline{\alpha}_o$, $2\underline{\alpha}$	(vector) angular direction functions
$\underline{\alpha}_\perp$	(x, y) components of α
B, B_T	beam pattern parameters
b	$\cos\theta_{oT} + \cos\theta_R = 2\alpha_z$
b_o	$\cos\theta_{oT} + \cos\theta_{oR} = 2\alpha_{oz}$
$\langle\,\rangle$	statistical average
c_o	(min.) wave propagation speed in water
C	beam projection dyadic
δ	delta function
$\underline{\hat{D}}$	surface dyadic
$F^{(o)}$	TSSF = total surface spreading function
F_1, F_2	characteristic functions
$\underline{\mathcal{F}}$	fourier transform operator
f_s	wave frequency
$G^{(1)}$, $\hat{G}^{(1)}$, $\hat{G}^{(2)}$	geometric factors, with absorption
g	gravitational acceleration; (also, subscript)
g_T, g_R	aperture gain factors
G	gravity-capillary wave surface

$H^{(12)}_{coh}$, $H^{(12)}_{inc}$	angular parameters of the NSCF
I_1, I_2, I_3	beam integrals
$\hat{\underline{I}}$	unit dyadic
$\hat{\underline{i}}_x$, $\hat{\underline{i}}_y$, $\hat{\underline{i}}_z$, $\hat{\underline{i}}_{oR}$, $\hat{\underline{i}}_{oT}$, $\hat{\underline{i}}_R$	unit vectors
K_a, K_S	directional covariances
K_{o-in}	intensity of applied signal
$\underline{K}$, $\underline{K}_S$	(vector) wave numbers
k, k_o, $\underline{k}$, $\underline{k}_D$	wave numbers
$\underline{L}_o$, $\underline{L}_1$, $\underline{L}_2$	horizontal separation of source and receiving point
L_S	spatial duration of soliton
L_o, $L_{1,2}$	(horizontal) separation between source and receiver, points of observation
ℓ_c, ℓ_S, ℓ_g	(horizontal) correlation distances
λ_o	acoustic wavelength in water
$M^{(12)}_a$, $M^{(12)}_{\langle a \rangle}$	spatial coherence functions
$\hat{m}^{(12)}_{coh}$, $\hat{m}^{(12)}_{inc}$	NSCF's
NSCF	normalized surface coherence function
$N^{(12)}_{GS}$, $N^{(12)}_{Gc}$	"tilt" factors
$N^{(o)}_{GS}$, $N^{(o)}_{Gc}$	"tilt" factors
$\hat{\underline{n}}$	unit normal
$\hat{\underline{n}}_G$	unit normal to surface G
ω_o, ω_s	angular frequencies
ϕ_{oT}, ϕ_{oR}	beam angles
ϕ_T, ϕ_R	beam pattern phases

ϕ_{oL}, ϕ_{L1}, ϕ_{L2}	angles of $\underline{L}_o$, $\underline{L}_1$, $\underline{L}_2$
ϕ_ν	angular direction of wave number vector
$R_G \doteq R_g$	Raleigh numbers
R_{oT}, R_{oR}	source and receiver distances
R, R_1, R_2	spatial distance
$\mathcal{R}_o$	plane-wave reflection coefficient
ΔR	path difference
$\underline{r}$	$\underline{i}_x x + \underline{i}_y y$ = vector in (x,y)-plane
ρ_S	normalized covariance of soliton
ρ_w	density of water
S_o	reference surface
$S_{in}(s)$	input signal spectrum
$\bar{S}$, $\overline{S^2}$	(moments of) shadowing function
s	complex (angular) frequency
$\hat{\sigma}(0)$	scattering cross section
S	(subscript) soliton component
SCF	surface coherence function
σ_h	(rms) correlation length of soliton ensemble
σ_g^2, σ_c^2, σ_G^2, σ_S^2	mean square wave heights
σ_{gx}^2, σ_{Gx}^2	mean square wave slopes
$\hat{\sigma}_{coh}(0)$, $\hat{\sigma}_{inc}(0)$	scattering cross-sections
T_o	path delay
$\mathcal{J}$	surface tension constant
θ_{oT}, θ_{oR}	beam angles
θ_{R1}, θ_{R2}	vertical angles of observation

t, t_1, t_2	time variables
τ, τ	time delay, time difference
U_∞	reference near-surface (mean) wind speed
W_G, W_g, W_c, W_S	directional surface wave number intensity spectra
W, $W_{g,c}$	point spectrum of surface waves
w_S, w_G	normalized wave number spectra
ζ, ζ_c, ζ_g, ζ_G, ζ_S	wave surface elevations
ζ_x, ζ_y, ζ_{gx}, ζ_{Gx}, etc.	derivatives of surface elevation (e.g., slopes)

ACOUSTIC SCATTERING FROM COMPOSITE WIND-WAVE SURFACES III: FORWARD SCATTER INTENSITIES AND SPATIAL COHERENCE AT LOW AND HIGH FREQUENCIES AND SMALL GRAZING ANGLES FOR "BUBBLE-FREE" RÉGIMES†*

by

David Middleton**

PART I: FORMULATION AND RESULTS

1. INTRODUCTION

The author's earlier work on high-frequency, small-angle underwater acoustic scattering from wind-wave surfaces has been largely developed in [1] and [2]. These references contain the detailed analytic structure which we shall specialize here to selected forward scattering problems (I) and spatial coherence measures (II), now for both low and high frequency régimes. The general aim of this study is to provide analytic results which can assist the design and interpretation of a variety of current experiments. For the scattering portion (I) of this study, we seek (forward) scattering intensities for both the received coherent and incoherent surface scatter components. For measures of the coherence properties of the surface scattered field (II), we shall examine the spatial covariance function of that field.

---

† This is Part III, continuing the author's earlier studies:
(i) "Acoustic Scattering for Truly Composite Wind-Wave Surfaces: Scattering Without Bubbles, NUSC Tech. Doc. TD-7205, 20 August 1984, NUSC, New London, CT 06320 (Ref. [1] here).
(ii) "Acoustic Scattering from Composite Wind-Wave Surfaces II: Backscatter Cross-Sections and Doppler Effects at High Frequencies and Small Angles for "Bubble-Free Régimes," NUSC Tech. Report TR-7635, 22 July 1986, NUSC, New London, CT 06320 (Ref. [2] here).

*Work supported under contract N66604-85-M-C456 with the Naval Underwater Systems Center (NUSC), New London, CT 06320.

**Contractor, Physics and Applied Mathematics, 127 E. 91st, New York, NY 10128.

As before in [1] and [2], we shall require an additional wave surface component, namely, the nonlinearly wind-generated random soliton surface layer, which to date appears the most promising mechanism to account for the observed backscatter and doppler data [3]-[7] of recent, precise experiments involving near-surface "bubble-free" régimes [8]; (see also, other supporting data described in [4], [6a], and [7]). In this analysis, we shall use the more recent versions of the soliton-surface model, which yield spectra and intensities in good agreement with observation (cf. secs. 3.1, 5.1 of [4]; sec. 5.2 of [6a]). In addition, experiments associated with the present analytical model can help to further identify and quantify the soliton-surface component, which so far has only been inferred from a broad variety of data [4]-[7].

The desired analytic results are from Problem (I): forward surface scatter cross-sections, at both Snell and off-Snell angles, for coherent and incoherent scatter and small angles $O(\lesssim 25°)$, and at both "high" and "low" frequencies. By the latter is meant, respectively, large and small Rayleigh numbers, R_g, which translates practically into a central emission frequency f_o which is here $O(\geq 5$ kHz) and O(0.2-2.0 kHz), respectively.* For Problem (II), spatial coherence of the forward surface scatter fields, as seen in the volume, we obtain the spatial covariance function for both the coherent and incoherent components of this field. This, in turn, permits us directly to determine a correlation distance as a practical measure of spatial coherence.

In all the above, we operate in the far-field, or Frauenhofer region, vis-à-vis the scattering region of the wind-wave surface, and employ coherent narrowband signals as before [1], [2]. Moderate to strong near surface winds, U_∞ = O(5-15 m/s), are also assumed, appropriate to the generation of the soliton surface layer [3]-[5], [6b] postulated here. Coupling to the medium involves a narrow-beam (large-aperture) parametric source (T), with either a narrow-beam or omnidirectional receiving beam (R) as before [1].

---

*The present Kirchoff (or tangent-plane) analysis [used in [1], [2], also] applies for $f_o \gtrsim O(200$ Hz), while the perturbational method is more suited to the lower frequencies, and presents problems at $f_o \gtrsim O(2$ kHz). For details, see the remarks in E, Appendix A.1.

Accordingly, this report is organized as follows: Section 2 provides a short summary and discussion of the principal results; Sections 3 through 5 (Part II) comprise an Analytical Summary, respectively, for results of the scattering cross-sections and the scattered field covariances, which in turn are the basis for the remarks in Section 2. For full technical details and derivations, the reader is referred to [1] (and to [4] and [5] for the solition surface model).

2. SUMMARY AND DISCUSSION OF RESULTS

The main results of this investigation are presented here in a generally descriptive form. The technical details, derivations and cross-section formulae are, for the most part, provided in Part II following. We consider first a short discussion of Problem I, which is concerned with forward scatter cross-sections at small grazing angles. "Forward" here means, geometrically forward in the yz-plane (cf. Fig. 3.1) of the receiver (R), transmitter (T), and z-axis ($\phi_{oL} = \pi/2 = \phi_{oT}$). We also consider "oblique" scattering, including oblique forward scatter ($\phi_{oL} \neq \pi/2$, $\phi_{oT} = \pi/2$), where the receiver is not in the vertical plane of the transmitter and the center (O_S) of the illuminated surface, cf. Fig. 3.1 again.

Let us note the following general results on a per-case basis (cf. Secs. 3, 4 ff.), as represented by the appropriate scatter cross-sections $\hat{\sigma}^{(0)}_{coh}$, $\hat{\sigma}^{(0)}_{inc}$, remembering that the grazing angle (of the transmitter) is small $0(5°) \leq \phi \leq 0(25°)$.

Case 1: High-Frequency, Coherent Scatter Eq. (3.4) [$f_o \geq 0(5\ kHz)$]; Sec. 4.1

This scatter contribution is usually totally ignorable because of (i) surface roughness ($R_g >> 1$) and (ii) oblique receiver orientation (α_{ox}, $\alpha_{oy} \neq 0$). An important exception occurs for forward scatter in the Snell direction ($\alpha_{ox} = \alpha_{oy} = 0$; $\alpha_{oz} = \cos \theta_{oT}$) where in spite of surface roughness a potentially observable coherent component may occur (cf. Sec. 4.1 ff.). The scatter cross-section in this instance is proportional to k_o^2 (cf. (3.4)).

Case 2: High-Frequency Incoherent Scatter Eq. (3.1) [$f_o \geq O(5\ kHz)$]; Sec. 4.2

Here the incoherent scatter component in the forward ($\phi_{oL} = \pi/2 = \phi_{oT}$) but off-Snell direction can be quite noticeable [O(-30 to -20 dB) for a typical situation, cf. Sec. 4.2]. In the Snell-direction, this component can be considerably larger, due primarily to the very large contribution of the gravity-wave component of the scattering surface, cf. (4.9). The depressing effects of surface roughness on the coherent contribution (Case 1) account for the significantly larger effects of the incoherent term here. Because of the high-frequency structure of the (soliton) surface wave number spectrum ($W_2 \sim k_o^{-4}$), cf. (3.16), the incoherent scatter cross-section becomes gradually independent of k_o as the signal frequency is increased [(3.16), (3.20) or (3.1) ff.].

Case 3: Low-Frequency Coherent Scatter Eq. (3.6) [$f_o \leq O(1\ kHz)$]; Sec. 4.3

In this instance, surface roughness is ignorable, but at oblique angles of observation the coherent forward scatter is once more vanishingly small, cf. Case 1 above. Again, in the Snell direction a significant coherent component may be expected O(20 dB), cf. (4.11), much larger than that of the corresponding high-frequency cases (Case 1) because of ignorable surface roughness.

Case 4: Low-Frequency Incoherent Scatter Eq. (3.5) [$f_o \leq O(1\ kHz)$]; Sec. 4.4

Here the forward, off-Snell scatter cross-section (with $\alpha_{ox} = 0$, $\alpha_{oy} \neq 0$), cf. (4.13), is noticeably larger than the on-Snell one (4.15), mainly because in our present model the large-scale gravity component makes no contribution, since then $\alpha_{ox} = \alpha_{oy} = 0$. In any case, this incoherent scatter is O(-50 dB to -80 dB), which is quite ignorable vis-à-vis the corresponding coherent component, cf. Case 3, above. Oblique scattering reduces the cross-section versus the off-Snell cases.

Included in our analysis is a summary of point-intensity and wave-number spectra of the gravity, capillary, and soliton layer components, Sec. 3.3 ff.

For Problem II, spatial coherence measures of the surface scattered field, we use the results of Sec. 5, in suitably normalized form, cf. Sec.

5.3. Thus, we have the following normalized spatial coherence functions (NSCF's), based on (5.24) and (5.25) ff., which we summarize as above in four cases:

Case 1: High-Frequency Coherent NSCF [$f_o \geq O(5\ kHz)$; Sec. 5.2A]

Using (5.11) in (5.24) gives for the (far-field) coherent NSCF, whose geometry is described by Fig. 5.1.

$$\hat{m}^{(12)}_{coh} \doteq H^{(12)}(\underline{\alpha}_1, \underline{\alpha}_2; k_o)_{coh} \left(1+\frac{R_1}{R_{oT}}\right)\left(1+\frac{R_2}{R_{oT}}\right) e^{-a_o c_o^2 k_o^2 |\Delta R|} \cos k_o \Delta R\,, \qquad \Delta R \equiv R_2 - R_1 \tag{2.1}$$

where

$$H^{(12)}_{coh} \equiv \bar{R}_o^2 \frac{\bar{S}^2 k_o^2 \mathcal{A}_1 \alpha_{1z}\alpha_{2z}}{2\pi^2} e^{-(R_{g1}+R_{g2})/2}\, e^{-\frac{k_o^2}{2}\left[2\underline{\alpha}_1\cdot\hat{\underline{C}}^{-1}\cdot 2\underline{\alpha}_1 + 2\underline{\alpha}_2\cdot\hat{\underline{C}}^{-1}\cdot 2\underline{\alpha}_2\right]} \tag{2.2a}$$

with $\underline{\alpha}_1$, $\underline{\alpha}_2$ given by (5.3d), namely

$$2\underline{\alpha} = \hat{\underline{i}}_x\left[\left(1+\frac{R_{oT}}{R}\right)\cos\phi_{oT}\sin\theta_{oT} - \frac{L}{R}\cos\phi_L\right] + \hat{\underline{i}}_y\left[\left(1+\frac{R_{oT}}{R}\right)\sin\phi_{oT}\sin\theta_{oT} - \frac{L}{R}\sin\phi_L\right] + \hat{\underline{i}}_z\left(\cos\theta_{oT}+\cos\theta_R\right) \tag{2.2b}$$

and,

$$2\alpha_{1z} \equiv b_1 = \cos\theta_{oT} + \cos\theta_{R1}\,, \text{ etc.};\quad R_{g1} \equiv \left(2\alpha_{\tilde{z}1}\sigma_G k_o\right)^2;\quad \hat{\underline{C}}^{-1} = \begin{bmatrix} A^{-1} & 0 \\ 0 & B^{-1}\end{bmatrix};\quad \underline{\alpha} = \underline{\alpha}_\perp, \tag{2.2c}$$

cf. (5.3 d,e) (5.10a), etc., $2\underline{\alpha}\cdot\hat{\underline{C}}^{-1}\cdot 2\underline{\alpha} =$ (5.10a), with R_g again the Rayleigh number for the gravity-wave component, cf. (3.4) et seq.

First, we note that when $R_1 = R_2 = R_{oR}$, and $\phi_{L1} = \phi_{L2}$, so that $P(\vec{R}_1) = P(\vec{R}_2)$ and $\therefore \Delta R = 0$, $2\underline{\alpha}_1 = 2\underline{\alpha}_2 = 2\underline{\alpha}_o$: the two points of observation coincide, and the NSCF $\hat{m}^{(12)}_{coh}$ reduces to the coherent scattering cross-section

$$\hat{m}^{(12)}_{coh}\Big|_{\substack{\vec{R}_1=\vec{R}_2,\text{ or}\\ \{\phi_{1L}=\phi_{2L};\,R_1=R_2\}}} = \hat{\sigma}^{(10)}_{coh}\,,\ \text{Eq (3.4), viz.}$$

$$\hat{m}^{(12)}_{coh}\Big|_{\{\}} \doteq \bar{R}_o^2\bar{S}^2\left(1+\frac{R_{oR}}{R_{oT}}\right)^2 \frac{\mathcal{A}_1 k_o^2 \alpha_{oz}^2}{2\pi^2}\, e^{-R_g}\cdot e^{-k_o^2\left[(2\nu_{ox})^2/A + (2\nu_{oy})^2/B\right]}, \tag{2.3}$$

as required by the geometry and physics of the situation.

At the Snell angle we require either one or both of the observation points to obey the Snell configuration $(\alpha_x = \alpha_y)_{1,2} = 0$, $(\alpha_z)_{1,2} = \cos\theta_{oT}$. If only one point is at the Snell angle, then H_{coh} is vanishingly small, because A, B are again small in (2.2a) for the other point ($\underline{\alpha}_\perp \neq 0$), and thus $\hat{m}^{(12)}_{coh} \doteq 0$, further decreased by the large Rayleigh numbers here. Similar remarks apply at oblique angles, where $\underline{\alpha}_{|1\perp|}$, $\underline{\alpha}_{2\perp} \neq 0$. On the other hand, when both points ($R_1 \neq R_2$) are at the Snell angle $(\alpha_x = \alpha_y)_{1,2} = 0$; $\alpha_z = \cos\theta_{R1} = \cos\theta_{R2} = \cos\theta_{oT}$, the frequency-dependent exponent in (2.2a) vanishes, cf. (2.6) and (2.9b,c) ff., but now the surface roughness effects dominate, and once more $\hat{m}^{(12)}_{coh} \to 0$, paralleling the behavior of the coherent scattering cross-section, noted in Case 1, Problem I above.

The spatial behavior of $\hat{m}^{(12)}_{coh}$ exhibits a characteristic damping due to path absorption, which, however, is usually quite small unless ΔR is very large. In addition, there is an oscillatory component, $\cos k_o \Delta R$, stemming from the different path delays along $\underline{R}_1$ and $\underline{R}_2$, cf. Fig. 5.1. There is also a "distance" or "mirror" factor $(1 + R_1/R_{oT})(1 + R_2/R_{oT})$, which stems from the definition of $\hat{m}^{(12)}_{inc}$, cf. (5.24). Finally, for oblique scattering ($\phi_{1L} \neq \phi_{2L}$), $\hat{m}^{(12)}_{coh}$ is also ignorable, similarly because of surface roughness and the frequency-dependent obliquity terms in the exponent of (2.2a), (2.3).

Case 2: High-Frequency Incoherent NSCF [$f_o \geq O(5\text{ kHz})$; Sec. 5.2b]

Applying (5.21) to our definition (5.25) for the NSCF gives directly

$$\hat{m}^{(12)}_{inc} \doteq H^{(12)}(\underline{\alpha}_1, \underline{\alpha}_2; k_o)_{inc}\, e^{-a_o k_o^2 c_o^2 |\Delta R|} \cos k_o \Delta R \cdot$$
$$\cdot \left\{ \frac{A_{1\alpha} A_{2x}\, e^{-k_o^2 \sigma_G^2 (b_1 - b_2)^2}}{b_1 b_2 \sigma_{Gx} \sigma_{Gy}} \cdot e^{-\frac{1}{2}(\underline{\alpha}_1 + \underline{\alpha}_2)\cdot \hat{D}_{12}^{-1} \cdot (\underline{\alpha}_1 + \underline{\alpha}_2)} \cdot \frac{k_o^4}{16\pi^2} N^{(12)}_{GC\text{-}inc}\, W_c\left[(\underline{\alpha}_1 + \underline{\alpha}_2)_\perp k_o, 0\right] \right.$$
$$\left. + \frac{k_o^4}{16\pi^2} N^{(12)}_{GS\text{-}inc}\, W_s\left[(\underline{\alpha}_1 + \underline{\alpha}_2)_\perp k_o | 0\right] \right\}, \qquad (2.4)$$

where now

$$\begin{cases} H^{(12)}_{inc} \equiv \overline{R_o^2}\,\overline{S^2}\, e^{-k_o^2 \Delta\underline{\alpha}_\perp \cdot \hat{C}^{-1} \cdot \Delta\underline{\alpha}_\perp} \quad ; \quad b_1 = z_{\alpha_{1z}} \text{ etc.} \\ N^{(12)}_{GC\text{-}inc},\ N^{(12)}_{GS\text{-}inc} = \text{Eqs. (5.4a,b)} \end{cases} \qquad (2.4a)$$

$$A_{1\alpha,2\alpha} \equiv \left(\frac{\alpha_x^2+\alpha_y^2+\alpha_z^2}{\alpha_{z/2}}\right)_{1,2}, \quad (5.13a); \quad \hat{\underline{D}}^{(12)^{-1}} = \begin{bmatrix} \epsilon_{Gx}^{-2} & 0 \\ 0 & \epsilon_{Gy}^{-2} \end{bmatrix} (b_1 b_2)^{-1}, \quad (5.15a) \qquad (2.4b)$$

and $N_{Gc}^{(12)}$, etc. are the "tilt-factors" respectively associated with the capillary and soliton-layer components, where in (2.4) W_c, W_S are wave-number intensity spectra. Equation (2.4) is the general high frequency form of $\hat{m}_{inc}^{(12)}$, the incoherent NSCF. The wavenumber $k = |(\underline{\alpha}_1 + \underline{\alpha}_2)_\perp| k_o$ is obtained explicitly with the help of (2.2b), where $|(\underline{\alpha}_1 + \underline{\alpha}_2)_\perp| = \sqrt{(\alpha_{1x} + \alpha_{2x})^2 + (\alpha_{1y} + \alpha_{2y})^2}$.

In our present applications, where the grazing angle is small ($\phi = \pi/2 - \theta_{or}$) is $O(\leq 25°)$; [in fact, usually ϕ is 10°], the first term of (2.4) effectively vanishes, except possibly at the Snell angle when $\underline{R}_1 \neq \underline{R}_2$, or when $P(\underline{R}_1)$ and $P(\underline{R}_2)$ coincide, i.e., we have the situation where $\hat{m}_{inc}^{(12)} \to \hat{\sigma}_{inc}^{(0)}$, cf. Problem I, Case 2, above. Moreover, at moderate (or above) wind speeds $\bar{U}_\infty > O(5$ m/sec), the soliton surface layer is expected to be present [4], [6a,b], [7], so that $W_S >> W_c$, and (2.4) accordingly reduces here to

$$\hat{m}_{inc}^{(12)} \doteq H_{inc}^{(12)} e^{-a_o k_o^2 c_o^2 |\Delta R|} \cos k_o \Delta R \left\{ \frac{k_o^4}{16\pi^2} N_{GS\text{-}inc}^{(12)} W_S\left[(\underline{\alpha}_1 + \underline{\alpha}_2)_\perp k_o | 0\right] \right\}. \qquad (2.5)$$

This, in turn, also reduces to the expected incoherent scatter cross-section $\hat{\sigma}_{inc}^{(0)}$ when $P(\underline{R}_1) = P(\underline{R}_2)$, cf. Figs. 3.1 and 5.1.

At the Snell angle when $R_1 \neq R_2$, but $\theta_{R1} = \theta_{R2} = \theta_{oT}$, then $\phi_{oT} = \pi/2 = \phi_{L1} = \phi_{L2}$, so that $b_1 = b_2$ and $\underline{\alpha}_{1\perp} = \underline{\alpha}_{2\perp} = 0$, cf. (2.2b), which requires the following relationship between the distances involved, viz.

$$\frac{R_1 + R_{oT}}{R_2 + R_{oT}} = \frac{L_1}{L_2} \qquad (2.6)$$

[When $R_1 = R_2$ here, of course, the observation points coincide and $\hat{m}^{(12)}_{inc} = \hat{\sigma}^{(0)}_{inc}$, namely

$$\hat{\sigma}^{(0)}_{inc} \doteq \overline{R_o^2}\,\overline{S^2}\,\frac{k_o^4}{16\pi^2}\,N^{(0)}_{GS\text{-}inc}\,W_S(2\underline{\alpha}_{o\perp}k_o\,|\,0), \tag{2.7}$$

cf. (3.1) and (4.5).]

The incoherent NSCF (2.5), unlike the coherent NSCF (2.1) above, depends only on the path distance difference ΔR (apart from the R_1, R_2-dependence exhibited in the directional angles $2\underline{\alpha}_{1,2}$, (2.2b)). Again, the absorption effects may be neglected as long as ΔR is not excessively large and only the spatial oscillatory component $\cos k_o \Delta R$ remains. The NSCF is much smaller at oblique angles than in the dual Snell cases ($\phi_{oT} = \pi/2 = \phi_{L1} = \phi_{L2}$; $\theta_{R1} = \theta_{R2} = \theta_{oT}$), paralleling similar behavior for the incoherent scatter cross-section [(2.3) et seq.].

Case 3: Low-Frequency Coherent NSCF [$f_o \leq$ O(1 kHz); Sec. 5.2A]

The formulae and results of Case 1, Eq. (2.1) et seq., apply here, except that surface roughness now plays a negligible rôle in depressing the magntiude of $\hat{m}^{(12)}_{coh}$: Equation (2.2a) applies, with $R_{g1} \doteq R_{g2} \doteq 0$.

Thus, (2.2a) becomes

$$H^{(12)}_{coh\,|\,low\text{-}freq} \doteq \overline{R_o}^2\,\overline{S}^2\,\mathcal{A}_1\,\frac{\alpha_{1z}\alpha_{2z}}{2\pi^2}\,e^{-\frac{k_o^2}{2}\left[2\underline{\alpha}_1\cdot\hat{\underline{C}}^{-1}\cdot 2\underline{\alpha}_1 + 2\underline{\alpha}_2\cdot\hat{\underline{C}}^{-1}\cdot 2\underline{\alpha}_2\right]} \tag{2.8}$$

Oblique, or semi-Snell (i.e., only one $P(\underline{R}_1)$ or $P(\underline{R}_2)$) at the Snell angle), reception still ensures a negligible coherent contribution for the NSCF, (2.1) and (2.3), while on the other hand, if $R_1 \neq R_2$ but both points of observation obey the Snell angle ($\phi_{1L} = \phi_{2L} = \phi_{oT} = \pi/2$) so that (2.6) is satisfied, then $\underline{\alpha}_{1\perp} = \underline{\alpha}_{2\perp} = 0$, $\alpha_{1z} = \alpha_{2z} = \cos\theta_{R1} = \cos\theta_{R2} = \cos\theta_{oT}$, and (2.1) reduces to

$$\hat{m}^{(12)}_{coh\,|\,\substack{low\text{-}freq\\ Snell}} \doteq \left(1+\frac{R_1}{R_{oT}}\right)^2\frac{L_2}{L_1}\,\overline{R_o}^2\,\overline{S}^2\,\mathcal{A}_1\,\frac{k_o^2\cos^2\theta_{oT}}{2\pi^2}\,e^{-q_o k_o^2 c_o^2|\Delta R|}\cos k_o\Delta R, \tag{2.9}$$

which is the extension of (2.3) to two separate points ($R_1 = R_2$) in the Snell plane. [When these points coincide, $R_1 = R_2 \to R_{oR}$, $\therefore L_2 = L_1 \to L_o$, and $\Delta R = 0$, and thus the low frequency result (2.9) reduces directly to

$$\hat{m}_{coh}^{(12)} \longrightarrow \hat{\sigma}_{coh}^{(0)}\Big|_{\substack{R_g \ll 1 \\ \text{Snell}}} \doteq \left(1 + \frac{R_{oR}}{R_{oT}}\right)^2 \bar{R}_o^2 \bar{S}^2 \mathcal{A}_1 \frac{k_o^2 \cos^2\theta_{oT}}{2\pi^2}, \tag{2.9a}$$

which is just (4.10) ff. without the factor $\exp(-R_g)$.]

In the Snell <u>high-frequency cases</u>, (2.9a) with (2.6) is slightly generalized to

$$\hat{m}_{coh}^{(12)} \longrightarrow \hat{\sigma}_{coh}^{(0)}\Big|_{\substack{R_g \gg 1 \\ \text{Snell}}} \doteq \left(1 + \frac{R_{oR}}{R_{oT}}\right)^2 \bar{R}_o^2 \bar{S}^2 e^{-R_g} \mathcal{A}_1 \frac{k_o^2 \cos^2\theta_{oT}}{2\pi^2} \longrightarrow 0, \tag{2.9b}$$

while (2.9) itself becomes ($R_1 \neq R_2$):

$$\hat{m}_{coh}^{(12)}\Big|_{\substack{R_g \gg 1 \\ \text{Snell}}} \doteq \left(1 + \frac{R_{oR}}{R_{oT}}\right)^2 \frac{L_2}{L_1} \bar{R}_o^2 \bar{S}^2 e^{-R_g} \mathcal{A}_1 \frac{k_o^2}{2\pi^2} \cos^2\theta_{oT} \longrightarrow 0. \tag{2.9c}$$

These quantities again vanish because of surface roughness: $\exp(-R_g) \to 0$.

<u>Case 4: Low-Frequency Incoherent NSCF [$f_o \leq O(1$ kHz); Sec. 5.2C]</u>

Finally, applying (5.23) to the definition (5.25) gives us directly for the low-frequency incoherent NSCF

$$\hat{m}_{inc}^{(12)}\Big|_{R_g \ll 1} \doteq H_{inc}^{(12)} e^{-4\sigma_o^2 k_o^2 c_o^2 |\Delta R|} \cos k_o \Delta R \cdot \left(\frac{k_o^4 b_1^2 b_2^2}{16\pi^2} W_g + \frac{k_o^4 N_{GG\text{-}inc}^{(12)}}{16\pi^2} W_c + \frac{k_o^4 N_{GS\text{-}inc}^{(12)}}{16\pi^2} W_S \right)_{(\underline{\alpha}_1 + \underline{\alpha}_2)_\perp k_o} \tag{2.10}$$

again with the tilt-factors $N^{(12)}_{Gc\text{-}inc}$, $N^{(12)}_{GS\text{-}inc}$ given by (5.4a,b) ff., and $b_1 = 2a_{1z}$, etc., cf. (2.4) above for the high frequency cases.

In the oblique or off-Snell directions ($\Delta\underset{\sim}{\alpha}_\perp \neq 0$), $H^{(12)}_{inc}$ is small, but not necessarily extremely so, so that (2.10) is dominated by $W_g\,[(\underset{\sim}{\alpha}_1 + \underset{\sim}{\alpha}_2)_\perp k_o | 0]$, the wave number spectrum of the gravity-wave component, cf. (4.13) ff. On the other hand, in the fully Snell casses, ($\phi_{oT} = \phi_{1L} = \phi_{2L} = \pi/2$), $\underset{\sim}{\alpha}_{1\perp} = \underset{\sim}{\alpha}_{2\perp} = 0$, $\alpha_{1z} = \alpha_{2z} = \cos\theta_{oT}$, $R_1 \neq R_2$, or $R_1 = R_2$, $W_g(0,0|0)$ vanishes, cf. (3.12a) ff., and (2.10) reduces to

$$\hat{m}^{(12)}_{inc}\Big|_{\substack{R_g \ll 1 \\ Snell}} \doteq \overline{R_o^2}\,\overline{S^2}\,e^{-a_o k_o^3 c_o^2 |\Delta R|} \cos k_o \Delta R \;\; \frac{(k_o \cos\theta_{oT})^4}{\pi^2} W_S\,[0,0|0), \tag{2.11}$$

cf. (4.14), with $W_S\,(0,0|0) = \pi\,\sigma_h^2\,\sigma_S^2$, vide (3.16), for the dominant soliton surface layer, which is comparable to the results of Case 4, Problem I. Equation (2.11) further reduces to $\hat{\sigma}^{(0)}_{inc}\big|_{R_g \ll 1,\ Snell}$ (4.14) here, when $\Delta R = 0$.

Further specialized developments of the results for Cases 1 through 4 here, for specific configurations and ocean surface states, may be made, based on these general results and on the analytical summary provided in Part II below.

PART II: ANALYTICAL SUMMARY

3. PROBLEM I: FORWARD AND OBLIQUE SCATTER CROSS-SECTIONS AT SMALL ANGLES

We apply at once the results of [1], in particular, Eqs. (2.13) and (2.24), to obtain, first, general results for scattering cross-sections in both the "high-" and "low-" frequency régimes of our study. In all cases, a Kirchoff rather than a perturbational approach is used, under far-field conditions, to include the effects of rather large slopes, cf. Sec. 5.4 et seq. of [1] and Chapter 10 of [9]. For derivation and technical details, see [1]. Specific references to the original results which form the basis of the present work are noted in what follows. Figure 3.1 here illustrates the general geometry.

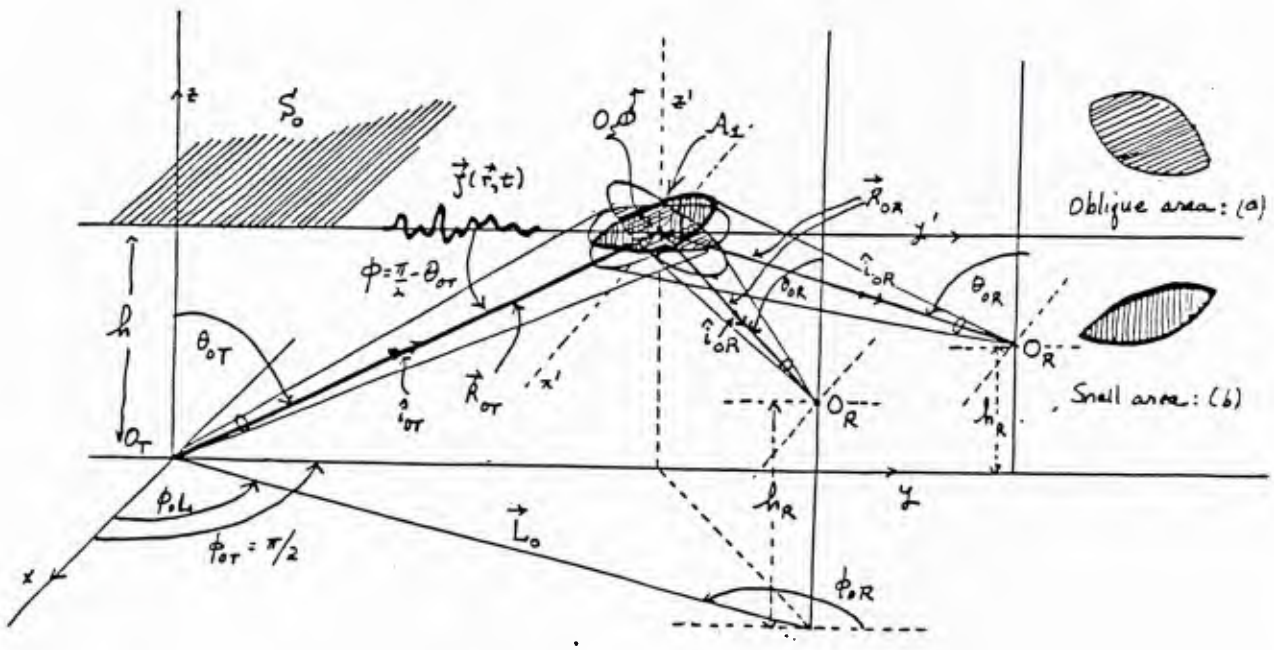

Figure 3.1. Bistatic scattering (R≠T): (a) forward oblique scattering; (b) forward scattering in the Snell direction; here $\phi_{oT} = \pi/2$; $\phi_{oR} \neq \pi/2$; $\zeta \neq$ surface elevation about $\langle\vec{\zeta}\rangle = 0$, at $z = h$. Here also, O_T, O_S, O_R are respectively the origin of the transmitter (T), scattering (S), and receiver (R) apertures.

3.1 HIGH-FREQUENCY SURFACE SCATTER CROSS-SECTIONS

From (2.13), [1] we write directly for the incoherent scatter cross-sections in the high-frequency régime ($R_g >(>) 1$), for arbitrary grazing angles ϕ ($= \pi/2 - \phi_{oT}$), it

(2.13), [1]:

$$\hat{\sigma}^{(0)}_{inc}\Big|_{R_g>(>1)} \simeq \overline{\mathcal{R}_o^2}\,\overline{\mathcal{S}^2}\left[\left\{\left(\frac{\alpha_{ox}^2+\alpha_{oy}^2+\alpha_{oz}^2}{\alpha_{oz}/2}\right)^2 \frac{e^{-\left[\frac{(2\alpha_{ox})^2}{\sigma_{Gx}^2}+\frac{(2\alpha_{oy})^2}{\sigma_{Gy}^2}\right]/2b_o^2}}{8\pi b_o^2\sigma_{Gx}\sigma_{Gy}} + \frac{k_o^4}{16\pi^2}N^{(0)}_{Gc\text{-}inc}\,W_c\left(2\underset{\sim}{\alpha}_o k_o|_{x,y},0\right)\right\}_G + \frac{k_o^4}{16\pi^2}N^{(0)}_{GS\text{-}inc}\,W_S\left(2\underset{\sim}{\alpha}_o k_o|_{x,y},0\right)\right] \tag{3.1}$$

with $k_o = 2\pi/\lambda_o = \omega_o/c_o$, where $\omega_o(=2\pi f_o)$ is the angular central frequency of the source and c_o is the (mean) phase speed of sound propagation in the water medium. Generally, cf. Appendix A.I,

(2.18), [1]:

$$\begin{aligned} 2\underset{\sim}{\alpha}_o &= 2\,\hat{\underset{\sim}{i}}_x\alpha_{ox} + 2\,\hat{\underset{\sim}{i}}_y\alpha_{oy} + 2\,\hat{\underset{\sim}{i}}_z\alpha_{oz} = \hat{\underset{\sim}{i}}_{oT} - \hat{\underset{\sim}{i}}_{oR} \\ &= \hat{\underset{\sim}{i}}_x\left\{\left(1+\frac{R_{oT}}{R_{oR}}\right)\cos\phi_{oT}\sin\theta_{oT} - \frac{L_o}{R_{oR}}\cos\phi_L\right\} \\ &\quad + \hat{\underset{\sim}{i}}_y\left\{\left(1+\frac{R_{oT}}{R_{oR}}\right)\sin\phi_{oT}\sin\theta_{oT} - \frac{L_o}{R_{oR}}\sin\phi_L\right\} + \hat{\underset{\sim}{i}}_z b_o\,, \end{aligned} \tag{3.2}$$

with

$$b_o \equiv \cos\theta_{oT} + \cos\theta_{oR}\,. \tag{3.2a}$$

In particular, for the "forward" geometry chosen here and defined by $\phi_{oT} = \pi/2$ and $\phi_{oL} = \pi/2$, i.e., T and R in the yz plane, we have, cf. Fig. 3.1.

$$2\underset{\sim}{\alpha}_o = \hat{\underset{\sim}{i}}_y\left[\left(1+\frac{R_{oT}}{R_{oR}}\right)\sin\theta_{oT} - \frac{L_o}{R_{oR}}\right] + \hat{\underset{\sim}{i}}_z b_o\,. \tag{3.2b}$$

The quantities $\mathcal{R}_o$ and $\mathcal{S}$ are respectively the plane-wave reflection coefficient (here = 1) and the "shadow function" variously defined; (see Sec. 7.4C, [1], for calculations of $\overline{\mathcal{S}}$ and $\overline{\mathcal{S}^2}$. Generally, $\overline{\mathcal{S}}$, etc., is nearly unity for ocean

surfaces, unless $\phi < 5°$. The $N^{(0)}$ in (3.1) are "tilt-factors," respectively, for the capillary (c) and soliton surface (S) components which become, again for $\phi_{oT} = \pi/2$, cf. Fig. 3.1:

$$\underline{(2.14b),\ [1]}: \quad N^{(0)}_{Gc\text{-}inc} \doteq 16\alpha_{oz}^2\left(\alpha_{oy}^2\sigma_{Gy}^2 + \alpha_{oz}^2\right) \qquad (3\text{-}3a)$$

$$\underline{(2.14a),\ [1]}: \quad N^{(0)}_{GS\text{-}inc} \doteq 16\left(3\alpha_{oy}^4\sigma_{Gy}^4 + 6\alpha_{oy}^2\sigma_{Gy}^2 + \alpha_{oz}^4\right) \qquad (3\text{-}3b)$$

$\sigma_{Gx}^2, \sigma_{Gy}^2 << 1$, $\phi_{oT} = \pi/2 = \phi_{oL}$

in which

$$\sigma_{Gx}^2 \equiv \langle \zeta_x^2 \rangle_G = \left\langle \left(\frac{\partial \zeta_G}{\partial x}\right)^2 \right\rangle ; \quad \sigma_{Gy}^2 = \left\langle \left(\frac{\partial \zeta_G}{\partial y}\right)^2 \right\rangle ; \quad \sigma_G^2 \equiv \langle \zeta_G^2 \rangle, \text{ etc.}, \qquad (3\text{-}3c)$$

are the mean square slopes of the gravity-capillary (G) surfaces $\zeta(\underset{\sim}{r},t)$, etc.

For the more general "oblique" geometry, where $\phi_{oL} \neq \pi/2$ $(0 \leq \phi_{oL} \leq \pi)$, $\alpha_{ox} \neq 0$, $(L \neq 0)$, shown also in Figure 3.1, Eqs. (3.2), (3.2a) apply. The tilt-factors (3.3a,b) now take the more general forms $(\phi_{oL} \neq \pi/2)$:

$$N^{(0)}_{Gc\text{-}inc} = 16\left\{\alpha_{ox}^2\sigma_{Gx}^2 + \alpha_{oy}^2\sigma_{Gy}^2 + \alpha_{oz}^2\right\}\alpha_{oz}^2 \qquad (3.3d)$$

and

$$N^{(0)}_{GS\text{-}inc} \doteq 16\left\{\left(3\alpha_{ox}^4\sigma_{Gx}^4 + 3\alpha_{oy}^4\sigma_{Gy}^4\right) + \left(6\alpha_{ox}^2\alpha_{oz}^2\sigma_{Gx}^2 + 6\alpha_{oy}^2\alpha_{oz}^2\sigma_{Gy}^2\right) + \alpha_{oz}^4\right\}. \qquad (3.3e)$$

The relations (3.3) apply for small slopes, here assumed to obey gaussian statistics, as does the surface elevation ζ, cf. Sec. 7.4B of [1]. These tilt-factors represent the effects of the large-scale gravity (g) wave component of the surface, which locally tilts the small-scale capillary (c) and soliton-surface (S) layer components, which "ride" upon the former.

Of course, the gravity-capillary surface (G) is physically one continuous surface $\zeta(\underset{\sim}{r},t)_G$, which it is analytically convenient to split into two separate components. Then, the expression in $\{\ \}_G$, (3.1), embodies the approximating dichotomy of the continuous surface into the g- and c-wave components: the first term (g) represents the so-called "physical optics" approximation while the second (c) is the small-scale capillary contribution. The third term represents the effects of the soliton-surface layer (S), which rides upon the gravity-capillary continuum [4], [5]. (The expression $2\underset{\sim}{\alpha}_o k_o|_{x,y}$ denotes the (x,y)-components of $2\underset{\sim}{\alpha}_o k_o$ in the usual way; this is also often written $2\underset{\sim}{\alpha}_{o\perp} k_o$.) Finally, W_c, W_S in (3.1) are respectively the wave number intensity spectra of the capillary and soliton components, whose specific form we shall consider in Sec. 3.3 following.

In similar fashion the associated <u>coherent scatter cross-section for all frequencies as well as in the high frequency régime</u>, again for arbitrary grazing angles ϕ, is found to be*

<u>(2.15), [1]</u>:

$$\overset{\wedge(o)}{\sigma}_{coh}\Big|_{\substack{R_o>(>1)\\ \text{all freq.}}} \simeq \overline{R}_o^2\,\overline{S}^2\left(\frac{R_{oT}+R_{oR}}{R_{oT}}\right)^2 \frac{A_1 k_o^2}{2\pi^2}\left\{\alpha_{oz}^2 e^{-R_\theta} \cdot e^{-4k_o^2\left[\alpha_{ox}^2/A + \alpha_{oy}^2/B\right]}\right\}, \tag{3.4}$$

---

*Equation (2.15) [1] is incomplete with an erroneous additional factor 2 in the denominator, and 3 is replaced by 4 in the exponent. This misprint, however, does not affect the subsequent results in [1]. The Tolstoy and Clay result for $\hat{\sigma}^{(o)}_{coh}$ ($=S_{coh}$), (6.61) of [16], differs by a factor $2\left(\frac{R_{oT}+R_{oR}}{R_{oT}}\right)^2$, which appears in our result (3.4). This difference stems from the different definition (A.1-1) of coherent scattering cross-section used here. The calculations of $\langle X\rangle^2$ are the same when we set $p_{T+C} = 4\pi p$ here.

where $R_g \equiv (b_o k_o \sigma_G)^2$ is explicitly the Rayleigh number of the ($g \doteq G$)-component of the scattering wave surface, cf. (3.2a) and (3.3c): $\sigma_G^2 \equiv \langle \zeta_G^2 \rangle \doteq \langle \zeta_g^2 \rangle$. The quantities A and B are given by

$$\underline{(2.11),\ [1]}: \quad A_1 = 2\pi\sqrt{AB} = 2A_{REF}\,; \quad A \equiv A_T/R_{oT}^2 + A_R/R_{oR}^2 \qquad (3.4a)$$

$$B \equiv a_T^2(\theta_{oT})A_T/R_{oT}^2 + a_R^2(\theta_{oT}|\ldots)A_R/R_{oR}^2 \ (\leq A)$$

cf. (6.17a), (6.11a), (6.12a) of [1], as well as (6.4) therein. Often, it is convenient for measuring purposes to use a "point" sensor, or omnidirectional beam at the receiver. Then $A_R = 0$ and A, B (3.4a) are modified accordingly. Thus, in all cases here, A_1 is an effective projected beam area on the scattering surface, cf. (6.52) and Sec. 6.5C of [1]. Since A and B are small, essentially because R_{oT}, R_{oR} are large, and since R_g is large, O(10), the coherent scatter cross-section is vanishingly small, unless transmitter and receiver are in the Snell position vis-à-vis the (mean) scattering surface, cf. (3.6) ff. e.g., $\alpha_{ox} = \alpha_{oy} = 0$. Even here, surface roughness essentially destroys coherence. The result is that for practical purposes, at sufficiently high frequencies, i.e., large R_g, there is no coherent scatter component, regardless of angle ϕ. Note also that the coherent scatter cross-section (3.4) depends on the area illuminated via A_1 (3.4a), as distinct from the incoherent cases (3.1), (3.5) ff., which are always area-independent.*

3.2 LOW FREQUENCY SURFACE SCATTER CROSS-SECTIONS

Again, we use the general results (2.24), (2.25) of [1] to write, for abritrary grazing angles, the incoherent scatter cross-section in the now "low-frequency" régime ($R_g(\langle)< 1$):

---

*Subject, of course, to the conditions noted in Appendix A.1.

(2.24), [1]:

$$\hat{\sigma}^{(o)}_{inc}\Big|_{R_g(\ell)<1} \doteq \overline{R_o^2}\,\overline{S^2}\,\frac{k_o^4}{16\pi^2}\left\{\left[k_o^4 W_g(2\underline{\alpha}_o k_o|_{x,y},0)+N^{(o)}_{Gc\text{-}inc}W_c(2\underline{\alpha}_o k_o|_{x,y},0)\right]_G + N^{(o)}_{GS\text{-}inc}W_S(2\underline{\alpha}_o k_o|_{x,y},0)\right\}, \tag{3.5}$$

where, as above, cf. (3.1), W_c, W_S are again the wave number intensity spectra of the capillary and soliton-layer components. Here W_g is the wave number intensity spectrum associated with the gravity-wave component of the underlying physically continuous gravity-capillary wave surface. Explicit structure for these spectra are presented in Sec. 3.3 following.

The corresponding low-frequency coherent scatter cross-section is given by (2.25), namely*

$$\hat{\sigma}^{(o)}_{coh}\Big|_{R_g(\ell)<1} \doteq \left(\frac{R_{oT}+R_{oR}}{R_{oT}}\right)^2 \overline{R_o}^2\,\overline{S}^2\,\frac{A_1 k_o^2}{2\pi^2}\left\{\alpha_{oz}^2 e^{-4k_o^2\left[\alpha_{ox}^2/A+\alpha_{oy}^2/B\right]}\right\}, \tag{3.6}$$

which is just (3.4) as expected, with $\exp(-R_g) \doteq 1$. Moreover, $|\overline{R}_o| \doteq \overline{S}^2 \doteq 1$ here, unless $\phi < O(5°)$. We observe that $\hat{\sigma}^{(o)}_{coh} \sim k_o^2$, while $\hat{\sigma}^{(o)}_{inc} \sim k_o^4\, W_{g,c,S}$ at small angles, cf. (3.4), (3.6) versus (3.1), (3.5). In Sec. 3.3 ff. we shall show that $\hat{\sigma}^{(o)}_{inc}$ is k_o^o (i.e., is independent of frequency) for the dominant spectral components at high frequencies.

---

*The factor k_o^2 was inadvertently omitted in Eqs. (2.25), (2.27). (2.28), (2.30), (2.31) of [1]. Note also the 3→4 and $4\pi^2 \to 2\pi^2$ therein. This has no effect on the results of the earlier work [1] and [2], since we are concerned there with the incoherent cases only, in as much as at high frequencies, $\hat{\sigma}^{(o)}_{coh\text{-}back} \doteq 0$ for the backscatter configurations treated therein.

3.3 SURFACE WAVE NUMBER SPECTRUM MODELS

The wave number intensity spectra appearing in our results (3.1) and (3.5) for the incoherent scattering cross-sections are obtained in the following models:

A. Gavity-Wave Surface:

(7.56), [1]: $$W_g(\underline{k}|0) = \frac{\pi}{2} g^{1/2} k^{-3/2} \mathcal{W}_1\left(f_s = \frac{1}{2\pi}\sqrt{kg}\right) \langle \delta(\phi_\nu - \hat{\alpha}) \rangle_{\hat{\alpha}} \qquad (3.7)$$

where W_g is the point-intensity spectrum, $k = |\underline{k}|$, ϕ_ν $(= \tan^{-1}(k_y/k_x)$ is the wave number direction associated with $k(=\sqrt{k_x^2+k_y^2})$, $\hat{\alpha}$ is the wave direction. Here, the dispersion law relating k and f_s, the wave frequency, is

$$\omega_s^2 = gk; \quad \omega_s = 2\pi f_s. \qquad (3.8)$$

The directional factor $\langle\delta\rangle_{\hat{\alpha}}$ is

$$\langle \delta(\phi_\nu - \hat{\alpha}) \rangle_{\hat{\alpha}} = w_1(\hat{\alpha} - \hat{\alpha}_o), \quad -\frac{\pi}{2} < \hat{\alpha} - \hat{\alpha}_o \leq \pi/2; = 0 \text{ , elsewhere,} \qquad (3.9)$$

in which α_o is the mean wind direction and w_1 is the pdf of wave-front directions. Usually, w_1 is approximated by [10]

$$w_1(\hat{\alpha}) = \frac{2}{\pi} \cos^2\hat{\alpha}, \quad -\pi/2 \leq \hat{\alpha} \leq \pi/2; = 0, \text{ elsewhere.} \qquad (3.10)$$

A common choice (but usually not the appropriate one at high wave frequencies $f_s = 0(\geq 3$ Hz), [4], Figs. 5.3, 5.4, 6.9) for W_g, is the Pierson-Moskowitz spectrum [11]

$$\mathcal{W}_g \doteq G\big|_{P\text{-}M} = \frac{C_o}{\omega_s^5} e^{-b\omega_s^{-4}}\,; \quad \left.\begin{aligned} C_o &= 8.10\cdot 10^{-3} \\ b &= 0.74 g^4/\bar{U}_\infty^4 \\ g &= 9.80\ m/s^2 \end{aligned}\right\}. \tag{3.11}$$

From (3.8), (3.10), Eq. (3.11) in (3.7) gives

$$W_g(\underline{k}|0)_{P\text{-}M} = \frac{\hat{C}_o e^{-0.74 g^2/k^4 \bar{U}_\infty^4}}{k^4}\cdot \cos^2(\hat{\alpha}-\hat{\alpha}_o)\quad ;\quad \hat{C}_o = 8.10\cdot 10^{-3} \tag{3.12a}$$

$$\doteq \frac{\hat{C}_o}{k^4}\cos^2(\hat{\alpha}-\hat{\alpha}_o)\,, \qquad \lambda < 4m, \bar{U}_\infty \geq 10\,m/s\,. \tag{3.12b}$$

As expected from dimensional arguments, $W_g(\underline{k}|0)$ is $O(k^{-4})$ here, also [12].

B. Capillary-Wave Surface:

(7.55), [1]: $$W_c(\underline{k}|0) = \frac{3k^{1/2}}{4a_c^{1/2}}\mathcal{W}_c(f_s = k^{3/2}/2\pi\sqrt{a_c})\langle\delta(\phi_r-\hat{\alpha})\rangle_{\hat{\alpha}}, f_s \geq 0\,, \tag{3.13}$$

where $a_c = \rho_w/\mathcal{T}$, ρ_w = density of water (grams/cm^3) and $\mathcal{T} \doteq 74$ = surface tension, dynes-cm. Now the dispersion law is

$$k = (a_c w_s)^{1/3},\ f_s \geq f_D \tag{3.14}$$

where f_D is some frequency above which the gravity-capillary surface is dominated by the short-wave capillary components. Thus, for f_D = 14.5 Hz, λ_D = 2.4 cm, from (3.14).

Using the P-M spectrum (3.11) in (3.13), with (3.14), gives

$$W_c(\underline{k}|0)_{P\text{-}M} \doteq \frac{3\hat{C}_0 g^2 a_c}{4k^7}\langle\delta(\phi_w-\hat{\alpha})\rangle_{\hat{\alpha}}\, e^{-0.74 g^4 a_c^2/k^6\bar{U}_{\infty}^4} \longrightarrow \left(\frac{C_0'}{k^7}\right)\cos^2(\hat{\alpha}-\hat{\alpha}_0), \qquad (3.15)$$

(where now the units are gram, cm, dyne). Empirical data, for example, Mitsuyasu [13] and Honda [14], also [4], Sec. [6a], [6b] shows, however, that (3.15) is not the dominant component at these wave frequencies, cf. Sec. 4.2 below.

C. Soliton-Surface Component:

From the author's recent work [4], [5] and [6], [7], the wave number intensity spectrum is found to be, in the so-called "semi-isotropic" cases [where $\underline{K}_S \cdot \Delta r = |\underline{K}_S|\,|\underline{\Delta r}| = K_S \Delta r$, cf. Sec. 3.2 of [4] and Sec. 3.2 of [5]]

$$\boxed{W_S(\underline{k}|0)_{ISO} = \frac{\pi\sigma_h^2\sigma_S^2}{\left[1+(k\sigma_h/2)^2\right]^2} \backsimeq 16\pi\left(\frac{\sigma_S}{\sigma_h}\right)^2\frac{1}{k^4}, \quad -\pi/2 \le \hat{\alpha}-\hat{\alpha}_0 \le \pi/2,} \qquad (3.16)$$

for "down-wind" directions only. Here

σ_h = an average correlation length of the soliton "wavelets";

σ_S = the rms height of the soliton-wave surface component. } (3.16)

From (3.2), (3.2a), the wave number $k(=|\underline{k}|)$ is given here for the "forward" direction by

$$\boxed{k = 2k_0\alpha_{0L} = k_0\left\{\left(1+\frac{R_{0T}}{R_{0R}}\right)\sin\theta_{0T} - \frac{L_0}{R_{0R}}\right\}, \quad \begin{matrix}\phi_{0T}=\pi/2,\\ \phi_{0L}=\pi/2\end{matrix}\ \text{cf. Fig. 3.1,}} \qquad (3.17)$$

or more generally, by

$$k = 2k_0\alpha_{0L} = k_0\sqrt{(2\alpha_{0x})^2+(2\alpha_{0y})^2}$$
$$= k_0\left\{\left(1+\frac{R_{0T}}{R_{0R}}\right)^2\sin^2\theta_{0T} - \frac{L_0}{R_{0R}}\left(1+\frac{R_{0T}}{R_{0R}}\right)\sin\theta_{0T}\cos(\phi_{0T}-\phi_{0L}) + \frac{L_0^2}{R_{0R}^2}\right\}^{1/2}. \qquad (3.17a)$$

when $\phi_{oL} \neq \pi/2$, cf. Fig. 3.1.

In the anisotropic cases, we can use (7.52 a,b), [1] to write

$$W_s(\underline{k}|0) = \int_{-\infty}^{\infty} K_s(\underline{\Delta r}, 0) e^{-i\underline{k}\cdot\underline{\Delta r}} d(\underline{\Delta r}) ; \quad \underline{\nu} = \underline{k}/2\pi ; \nu = |\underline{\nu}| ; \tag{3.18a}$$

$$= \frac{1}{2}\int_{-\infty}^{\infty} \mathcal{W}_s^{\circ}(f_s)\, \delta(|\underline{\nu}| - |\underline{k}|/2\pi) \frac{1}{\nu} \left|\frac{df_s}{d\nu}\right| \langle \delta(\phi_\nu - \hat{\alpha}) \rangle_{\hat{\alpha}} df_s , \quad f_s \geq 0 \tag{3.18b}$$

$$= \frac{\bar{c}_s}{2\nu}\left(\int_0^{\infty} \mathcal{W}_s^{\circ}(f_s)\, \delta(f_s - \bar{c}_s k/2\pi)\, df_s\right) \langle \delta(\phi_\nu - \hat{\alpha}) \rangle_{\hat{\alpha}} \tag{3.18c}$$

$$\therefore W_s(\underline{k}|0) = \frac{\pi \bar{c}_s}{k} \mathcal{W}_s^{\circ}\left(f_s = \frac{\bar{c}_s k}{2\pi}\right) \langle \delta(\phi_\nu - \hat{\alpha}) \rangle_{\hat{\alpha}} , \tag{3.18d}$$

where we have used $k_s = \omega_s/\bar{c}_s = 2\pi f_s/\bar{c}_s$ for these dispersionless solitons. Now, the point-intensity spectrum, based on both empirical data (Sec. 5.1, [4], also [6a]) and the theoretical model [4], is found to be (cf. Sec. 3.2, [5]]

$$\mathcal{W}_s^{\circ}(f_s) = \frac{\pi \sigma_h^2 \sigma_s^2/\bar{c}_s}{\left[1 + (\omega_s \sigma_h/2\bar{c}_s)^2\right]^{3/2}} . \tag{3.19}$$

Applying (3.19) to (3.18d) gives directly

$$W_s(\underline{k}|0)_{ANISO} = \frac{\pi^2 \sigma_h^2 \sigma_s^2 \langle \delta(\phi_\nu - \hat{\alpha}) \rangle_{\hat{\alpha}}}{k\left[1 + (k\sigma_h/2)^2\right]^{3/2}} \simeq \left.\begin{aligned} & 8\pi^2 \left(\frac{\sigma_s}{\sigma_h}\right)^2 \langle \delta(\phi_\nu - \hat{\alpha}) \rangle_{\hat{\alpha}} \cdot \frac{1}{k^4} \\ & = \frac{16\pi}{k^4}\left(\frac{\sigma_s}{\sigma_h}\right)^2 \cos^4(\hat{\alpha} - \hat{\alpha}_o) \end{aligned}\right\} -\pi/2 \leq \hat{\alpha} - \hat{\alpha}_o \leq \pi/2, \tag{3.20}$$

where (3.9), (3.10) may be used for the directional wave averages $\langle \delta \rangle_{\alpha}$.

The conversion of (3.20) to the "semi-isotropic" cases (3.16) formally requires the directional average to be

$$\langle \delta(\phi_\nu - \hat{\alpha}) \rangle_{\hat{\alpha}} = \sigma_h k \Big/ \pi\left[1 + (k\sigma_h/2)^2\right]^{1/2}, \quad -\pi/2 < \hat{\alpha} - \hat{\alpha}_o \leq \pi/2 , \tag{3.21}$$

which is uniform in $\hat{\alpha}$ "downwind," but depends for wave-frequency ($k = \omega_s/\overline{c}_s$) cf. (3.16). In any case, note that for large k, $W_S(\underset{\sim}{k}|0) \simeq k^{-4}$, as required.*

D. Surface Component Heights:

The rms heights σ_g, σ_c, σ_S of the composite surface components appearing in (3.1) and (3.5) are found from the following:

I. Gravity-wave component:

$$\left.\begin{aligned} \sigma_g^2 = \overline{\zeta_{g\doteq G}^2} &= \pi \int_0^\infty \mathcal{W}_g(f_s)\,df_s \\ &= \int_{-\infty}^{\infty} W_g(\underset{\sim}{k}|0)\,d\underset{\sim}{k}/(2\pi)^2 \end{aligned}\right\}, \tag{3.22}$$

which for the P-M spectrum (3.11) yields

$$\boxed{\sigma_g^2 = \frac{\hat{C}_o \overline{U}_\infty^4}{8(0.74)g^2} \doteq (1.42)10^{-5}\,\overline{U}_\infty^4 \;;\; \overline{U}_\infty = m/s.} \tag{3.23}$$

$$\boxed{\doteq (1.42)\cdot 10^3\ cm^2 \;@\; \overline{U}_\infty = 10\,m/s.} \tag{3.23a}$$

II. Capillary-wave component:

$$\sigma_c^2 = \frac{\hat{C}_o q^2}{8b}\left(1 - e^{-b/\omega_D^4}\right), \tag{3.24}$$

from (3.11) and the partition of the P-M point spectrum into gravity $f_s < f_D$ and capillary régimes $f_s \geq f_D$, cf. (3.14). For $f_o = 14.5$ Hz and $\therefore \lambda_D = 2.4$ cm, we have

$$\boxed{\sigma_c^2 = 10^{-7}\,\sigma_g^2,\ @\ \overline{U}_\infty = 10\,m/s.} \tag{3.24a}$$

As expected, $\overline{\zeta_c^2} \equiv \sigma_c^2$ is O(70 dB) less than $\sigma_g^2 \equiv \overline{\zeta_g^2}$ at $\overline{U}_\infty = 10$ m/sec.

---

*Of course, this characteristic k^{-4} fall-off must be replaced ultimately by a faster fall-off, in order to ensure physically finite rms surface slopes.

III. Soliton-surface component:

$$\sigma_S^2 = K_S(0.0), \text{ Eqs. (3.10), (3.13) of [5]}$$
$$= O(1/2 - 6\ \text{cm}^2),\ \bar{U}_\infty = 10\ \text{m/s} \qquad (3.25)$$

from empirical backscatter data, cf. Fig. 5.2 of [5] and Fig. 2.2 of [2].

E. Summary Remarks:

From the above it is clear that, depending on frequency and geometry, the gravity and/or soliton surface components are dominant, since $\sigma_g^2 >> \sigma_S^2 >> \sigma_c^2$. The needed wave number spectra are given by (3.12) and (3.16), or (3.20) in the directional cases. Equation (3.17) indicates the explicit dependence of wave numbers k on the geometry in question.

4. PROBLEM I: SOME SPECIFIC RESULTS

Using the general results of Section 3 above for these forward scatter cases, at both high- and low-frequencies, but always at "small" angles, $\phi \leq O(25°)$, we find directly the following specific results:

4.1 HIGH-FREQUENCY COHERENT COMPONENT

Here $\hat{\sigma}^{(0)}_{coh}$ is given by (3.4), which is vanishingly small now because $R_g = (b_o k_o \sigma_G)^2 >> 1$ and A, B, (3.4a) are small, with α_{ox}, $\alpha_{oy} \neq 0$ for oblique "viewing" of the acoustically illuminated surface in the manner of Fig. 3.1(b).

An important exception may occur, however, in the Snell direction, where $(\hat{\underline{\imath}}_{oT})_x = (\hat{\underline{\imath}}_{oR})_x$, $(\hat{\underline{\imath}}_{oT})_y = (\hat{\underline{\imath}}_{oR})_y$, e.g., $\phi_{oT} = \pi/2 = \phi_{oL}$ and $(1 + R_{oT}/R_{oR}) \sin\theta_{oT} = L_o/R_{oR}$, cf. (3.2). Thus, $(\underline{\alpha}_o)_x = (\underline{\alpha}_o)_y = 0$, and $b_o = 2\alpha_{oz} = 2\cos\theta_{oT}$, and the only component reducing the coherent forward scatter is then $\sim e^{-Rg}$ in (3.4). For $f_o = 20$ kHz, $\bar{U}_\infty = 10$ m/s., $\theta_{oT} = 80°$ ($\phi = 10°$), we find that $R_g = (2\frac{\omega D}{c_o}\sigma_G \cos\theta_{oT})^2 = [2 \cdot (82.8) \cdot 1.42 \cdot 10^{-1} \cdot 0.174]^2 =$

$(4.09)^2 = 16.74$ and $\therefore \exp(-R_g) = 5.4.10^{-8} = -73$ dB which may or may not be significant vis-à-vis the incoherent component in similar circumstances. For example, let us consider

$$\therefore \left\{ \begin{array}{l} f_o = 20 \text{ kHz};\ \theta_{oT} = 80^\circ\ (\phi = 10^\circ);\ \overline{U}_\infty = 10 \text{ m/sec}; \\ k_o = 82.8 \text{ rad/m};\ R_{oT} = R_{oR}\text{: } \underline{\text{Snell angle}};\ \overline{R}_o \doteq \overline{S} \doteq 1; \\ \qquad A_1 = 2\pi \cdot 10^3 \text{ m}^2. \end{array} \right\} \tag{4.1}$$

Then (3.4) becomes

$$\hat{\sigma}^{(0)}_{coh}\Big|_{R_g >> 1:\ \text{Snell}} \simeq \frac{1}{\pi} \cdot 10^3 k_o^2 \cos^2\theta_{oT} e^{-R_g} \tag{4.2}$$

$$= 6.1 \cdot 10^4 e^{-R_g} = 3.5 \cdot 10^{-3} = -24.5 \text{ dB}$$

which is to be compared with (4.9) below. The comparison shows that for this case, the coherent component is ~53 dB lower than the accompanying incoherent contribution, and may not be entirely ignorable.

4.2 HIGH-FREQUENCY INCOHERENT COMPONENT

This is obtained from (3.1), with the observation that since

$$\sigma^2_{G(x=y)} = (3.0 + 5.12\overline{U}_\infty)10^{-3}, \qquad \overline{U}_\infty = \text{m/sec}, \tag{4.3}$$

from Cox and Munk [15], where for $\overline{U}_\infty = 10$ m/sec, $\sigma^2_{G(x=y)} = 5.4 \cdot 10^{-2}$. Thus, at $\theta_{oT} = 80^\circ$, we have in the forward direction ($\phi_{oL} = \pi/2$) but off the Snell angle for the exponent of the leading term in (3.1), with say $R_{oT} = R_{oR} = L_o$ ($\phi_{oT} = \pi/2$)

$$\exp\left[\mathcal{L}_g(3.1)\right] = O\left[-\frac{1}{2}\left(\frac{2\sin\theta_{oT} - 1}{2\epsilon_{Gy}\cos\theta_{oT}}\right)^2\right] = -\frac{1}{2}\left(\frac{0.97}{1.88 \cdot 10^{-2}}\right)^2 = -1.33 \cdot 10^3, \tag{4.4}$$

which is totally negligable vis-à-vis the other components in (3.1). Moreover, $N^{(0)}_{gS\text{-}inc} = 16 \cdot (1.68)10^{-2}$, from (3.2e) of [1], for these parameters.

Using (3.16) in (3.1) gives, again

$$\hat{\sigma}^{(0)}_{inc}\Big|_{\substack{\text{forward}\\ \text{off-Snell}}} \simeq \overline{R_0^2}\,\overline{S^2}\,\frac{k_0^4}{16\pi^2}\,N^{(0)}_{\partial S\text{-inc}}\,\frac{\pi\sigma_R^2\sigma_S^2}{\left[1+\left(k\sigma_h/2\right)^2\right]^2}\,, \qquad k = k_0\left(2\sin\theta_{oT}-1\right), \tag{4.5}$$

for the oblique geometry of (4.4), i.e., $R_{oT} = R_{oR} = L_o$, and as usual $\overline{U_\infty}$ = 10 m/sec, mean wind speed.

At these high frequencies (here f_o = 20 kHz) and small grazing angles (θ_{oT} = 80°) we have now for (4.5)

$$\therefore\ \hat{\sigma}^{(0)}_{inc}\Big|_{\text{forward off Snell}} \left.\begin{array}{l} \simeq (9.90)\cdot 10^{-3} = -20 \text{ dB (Roderick)} \\ \simeq (1.63)\cdot 10^{-3} = -27.9 \text{ dB (Galubin)} \end{array}\right\} \text{Fig. (2.2) of [4],} \tag{4.6}$$

respectively for σ_S/σ_h = 2.0/5.0 and = 0.8/1.5, the Roderick and Galubin data, cf. [4], Fig. (2.2). [To these results (4.6a) should be added a "Kirchoff correction" 0 (2.5 dB), as well as for (4.2) above.] In any case, the incoherent forward scatter here is considerable, 0(-18, -25 dB), with a totally negligible coherent component.

For forward scattering in the Snell direction, however, we have $\alpha_{ox} = \alpha_{oy} = 0$, $\alpha_{oz} = \cos\theta_{oT}$, so that (3.1) reduces directly to

$$\hat{\sigma}^{(0)}_{inc}\Big|_{\substack{\text{Snell, } R_q>>1\\ \text{forward}}} \simeq \overline{R_0^2}\,\overline{S^2}\left\{\left(8\pi\sigma^2_{G(x,y)}\cos^4\theta_{oT}\right)^{-1} + \frac{k_0^4}{\pi^2}\cos^4\theta_{oT}\,W_S(0,0\,|\,0)\right\}, \tag{4.7}$$

since the soliton component dominates the capillary contribution, cf. (3.25) versus (3.24). Applying (3.16) to (4.7) gives now

$$\hat{\sigma}^{(0)}_{inc}\Big|_{\substack{\text{Snell, } R_q>>1\\ \text{forward}}} \simeq \overline{R_0^2}\,\overline{S^2}\left\{\left(8\pi\sigma^2_{G(x,y)}\cos^4\theta_{oT}\right)^{-1} + \frac{1}{\pi}\sigma_R^2\sigma_S^2 k_0^4\cos^4\theta_{oT}\right\}. \tag{4.8}$$

Numerical examples, using (4.1), (4.3) above, where f_o = 20 kHz, cos θ_{oT} = 0.174, $\sigma^2_{G(x=y)} = 5.4 \cdot 10^{-2}$, etc., yield

$$\hat{\sigma}^{(0)}_{inc}\Big|_{\substack{\text{Snell}\\ Rg>>1\\ \text{forward}}} \simeq \left\{ 8.10 \cdot 10^2 + \begin{pmatrix} 1.36 \cdot 10^{-2}: & \text{(Roderick [4], Fig. 2.2)} \\ 1.96 \cdot 10^{-4}: & \text{(Galubin [4], Fig. 2.2)} \end{pmatrix} \right\}$$

$$\simeq 8.1 \cdot 10^2 = 29.1 \text{ dB}, \qquad (4.9)$$

where the geometric (i.e., gravity wave) term clearly dominates. As expected, the incoherent forward scatter at oblique angles is much less than that in the Snell direction, while the coherent forward scatter in the Snell direction is 50.5 dB less than the incoherent contribution, (4.2) versus (4.9). Surface roughness at these high frequencies explains the large difference.

4.3 LOW-FREQUENCY COHERENT COMPONENT

Again, at oblique angles the coherent scatter component (3.6) is vanishingly small, even though $R_g = (0.207)^2 = 4.28 \cdot 10^{-2}$ at f_o = 1 kHz, θ_{oT} = 80°, $\overline{U_\infty}$ = 10 m/sec, so that $\exp(-R_g) = 0.96$.

On the other hand, as in the high frequency cases the behavior is quite different for forward scatter in the Snell direction, $\alpha_{ox} = \alpha_{oy} = 0$; $\alpha_{oz} = \cos\theta_{oT}$. Accordingly, (3.6) reduces to

$$\hat{\epsilon}^{(0)}_{coh}\Big|_{\substack{R_g \ll 1\\ \text{Snell}}} \doteq \left(\frac{R_{oT}+R_{oR}}{R_{oT}}\right)^2 \overline{\mathcal{R}}_o^2 \overline{\mathcal{S}}^2 A_1 e^{-R_g} \frac{k_o^2 \cos^2\theta_{oT}}{2\pi^2}\,; \quad (\phi_{oT} = \phi_{oL} = \pi/2). \qquad (4.10)$$

As above, setting $R_{oT} = R_{oR}$ and $A_1 = 2\pi \cdot 10^3 m^2$, cf. (4.1), at 1 kHz (e.g., k_o = 4.19 m^{-1}) and θ_{oT} = 80° with $\overline{\mathcal{S}}^2 = \overline{\mathcal{R}}_o^2 \doteq 1$ yields

$$\underline{R_g << 1}: \quad \hat{\sigma}^{(0)}_{coh}\Big|_{\text{Snell}} \doteq \frac{1}{\pi} \cdot 10^3 \cdot 0.96\, k_o^2 \cos^2\theta_{oT} = 1.62 \cdot 10^2 = 22.1 \text{ dB}, \qquad (4.11)$$

which is to be compared with (4.2) in the high frequency example. The comparative lack of surface roughness here results in a 46.6 dB increase in $\hat{\sigma}^{(o)}_{coh}$ vis-à-vis the high-frequency case, although the effect of the lower frequency is to provide a factor $(20)^2 = 400$ reduction in the former.

4.4 LOW-FREQUENCY INCOHERENT COMPONENT ($\phi_{oL} = \pi/2$)

Here (3.5) applies, where as noted above in Secs. 3.3D,E, we can omit the capillary component. Then (3.5) becomes $\underset{\sim}{k} \to \hat{\underset{\sim}{i}}_y \, 2\alpha_{oy}$, cf. (3.2b):

$$\hat{\sigma}^{(o)}_{inc}\Big|_{R_g \ll 1} \doteq \overline{R_o^2}\,\overline{S^2}\,\frac{k_o^4}{16\pi^2}\left\{b_o^4\, W_g(0, 2(\underset{\sim}{\kappa}_o)_y|0) + N^{(o)}_{GS\text{-}inc}\, W_S(0, 2(\underset{\sim}{\kappa}_o)_y|0)\right\}, \tag{4.12}$$

with $\phi_{oT} = \phi_{oL} = \pi/2$, cf. Fig. (3.1), and

$$2\alpha_{oy} = \left(1 + \frac{R_{oT}}{R_{oR}}\right)\sin\theta_{oT} - Lo/R_{oR}; \quad 2\alpha_{ox} = 0 \tag{4.12a}$$

again here, and $N^{(o)}_{GS\text{-}inc}$ is given by (3.36).

For the parameters of our forward-scatter example above (cf. Sec. 4.2) namely $R_{oT} = R_{oR} = L_o$, $\theta_{oT} = 80°$, $\overline{U_\infty} = 10$ m/sec, so that $N^{(o)}_{GS\text{-}inc} = 16(1.68)10^{-2}$, for $k = k_o(2\sin\theta_{oT} - 1)$, $k_o = 4.19\text{m}^{-1}$ or $f_o = 1$ kHz, where we use (3.12) and (3.16) for the respective wave number spectra, we find after some simple calculations that, with $\overline{R_o^2} = \overline{S^2} \doteq 1$, the incoherent scatter cross-section is now

$$\hat{\sigma}^{(o)}_{inc}\Big|_{\substack{\text{forward}\\ \text{off-Snell}\\ R_g \ll 1}} \doteq \left[1.31\cdot10^{-5} + \begin{Bmatrix}1.65\cdot10^{-6}\ \text{(Roderick)}\\ 1.98\cdot10^{-8}\ \text{(Galubin)}\end{Bmatrix}\right] \doteq 1.3\cdot10^{-5} = -48.9\ \text{dB};$$

$$-\pi/2 \le \hat{\alpha} - \hat{\alpha}_o \le \pi/2. \tag{4.13}$$

This is $O(20^2 = 400 = 26.0$ dB) less than the result (4.6), mainly as a result of the 20:1 reduction in frequency but also stemming from the fact that now the main contribution comes from the gravity-wave component, instead of the soliton layer, which dominates in the high-frequency cases, cf. (4.4), (4.5).

Finally, in the Snell direction where $\alpha_{ox} = \alpha_{oy} = 0$, $\alpha_{oz} = \cos\theta_{oT}$, $\hat{\sigma}^{(0)}_{coh}$ becomes

$$\hat{\sigma}^{(0)}_{inc}\Big|_{R_g<<1;\,Snell} \doteq \overline{R_o^2}\,\overline{S^2}\,\frac{k_o^4}{16\pi^2}\left\{4\cos^4\theta_{oT}\;W_g(0,0|0) + 16\cos^4\theta_{oT}\;W_s(0,0|0)\right\}, \tag{4.14a}$$

$$\doteq \overline{R_o^2}\,\overline{S^2}\,\frac{k_o^4\cos^4\theta_{oT}}{\pi^2}\left\{\frac{1}{4}W_g(0,0|0) + W_s(0,0|0)\right\}, \tag{4.14b}$$

$$\doteq \overline{R_o^2}\,\overline{S^2}\,\left(\frac{k_o\cos\theta_{oT}}{\pi}\right)^4\sigma_h^2\sigma_s^2, \tag{4.14c}$$

from (3.16), since $W_g(0,0|0) = 0$, cf. (3.12a). Again, as an example, using the parameters above we get

$$\hat{\sigma}^{(0)}_{\substack{inc/R_g<<1\\ Snell}} \doteq \left\{\begin{matrix}8.91\cdot10^{-8} = -70.5\text{ dB (Roderick)}\\ 1.07\cdot10^{-9} = -89.7\text{ dB (Galubin)}\end{matrix}\right\}, \quad -\pi/2 < \hat{\alpha} - \hat{\alpha}_o \le \pi/2. \tag{4.15}$$

This is much smaller than our result (4.13) for non-Snell forward scatter, principally because in the present model of the large-scale gravity component (3.12a), $W_g(0,0|0) = 0 < W_g(0, 2\alpha_{oy}k_o|0)$, cf. (4.12): the gravity-wave component makes no contribution at these low frequencies and Snell angle, unlike its counterpart (4.9) in the high-frequency régimes. Incoherent forward scatter is due primarily to the soliton-surface component (4.15).

5. PROBLEM II: SPATIAL COHERENCE MEASURES OF SURFACE SCATTERED FIELDS

Here we wish to obtain a measure of spatial coherence of the acoustic field (in the water medium, as before) scattered from the illuminated surface, in the manner of Fig. 5.1, cf. Fig. 3.1. Although our results will apply for all directions of observation, we are primarily interested in the spatial

coherence of the forward scattered field. Our measure of the spatial coherence of the scattered acoustic field, $a_I(\underset{\sim}{R},t)$, is the Spatial Coherence Function (SCF), defined by

$$M_a^{(12)}\,(\underset{\sim}{R}_1,\ \underset{\sim}{R}_2|\tau = 0)_{inc} \equiv \left\langle \overline{a_I(\underset{\sim}{R}_1,t)}\, a_I(\underset{\sim}{R}_2,t)^* \right\rangle \tag{5.1a}$$

where $\langle\ \rangle$ denotes the time average, as usual [17], and

$$M_{\langle a\rangle}^{(12)}\,(\underset{\sim}{R}_1,\ \underset{\sim}{R}_2|\tau\to\infty)_{coh} \equiv \left\langle \overline{a_I(\underset{\sim}{R}_1,t)}\ \overline{a_I(\underset{\sim}{R}_2,t)^*} \right\rangle \tag{5.1b}$$

respectively for the incoherent and coherent components of the scattered field, a_I. In practice, of course, we need at least a point-sensor at $\underset{\sim}{R}_1$ and $\underset{\sim}{R}_2$: for our purposes, this is equivalent to omnidirectional receiving beams with unity gain ($g_R = 1$), located at $\underset{\sim}{R}_1$ and $\underset{\sim}{R}_2$, cf. Fig 5.1. The measurement configuration for these two-point reception processes is shown in Fig. 5.2. [Here a suitable delay $\hat{\tau}$ is introduced, in either branch of the resulting cross-correlator, to bring $t_2 = t_1 = t$ in the product.]

We shall consider again far-field cases only, where

$$\pi L_{max}\ell_{max}/\lambda_o \ll R_1,\ R_2, \qquad R_{1,2} = |\underset{\sim}{R}_{1,2}| \tag{5.2}$$

in which ℓ_{max} is the maximum (rms) correlation distance of the illuminated surface A_1, and L_{max} is the maximum dimension of the transmitting aperture, cf. (iii) of A.1,E. In addition, we again employ "narrow beams," in the sense that the spatial geometry for $P(\underset{\sim}{R}_1)$ and $P(\underset{\sim}{R}_2)$ change little over the illuminated region A_1 (cf. remarks Eq. (5.25) ff., p. 58 of [1]). When the small-scale surface component, namely the soliton surface layer, is dominant, which may be expected at high frequencies and small angles, these coherence points may be comparatively close to the illuminated wave surface in absolute terms. For example, at $f_o = 20$ kHz, then $\lambda_o = 7.5$ cm in water, and typically $\ell_{max} = \sigma_h \sim O(5\text{ cm})$, cf. (4.6), et seq., while $L_{max} = 50$ cm is typical. Then $R_1,\ R_2 \gg 1$ m, say 20m, from O_S in A_1, Fig. 5.1. The other conditions of Appendix A.1 E, F apply as before.

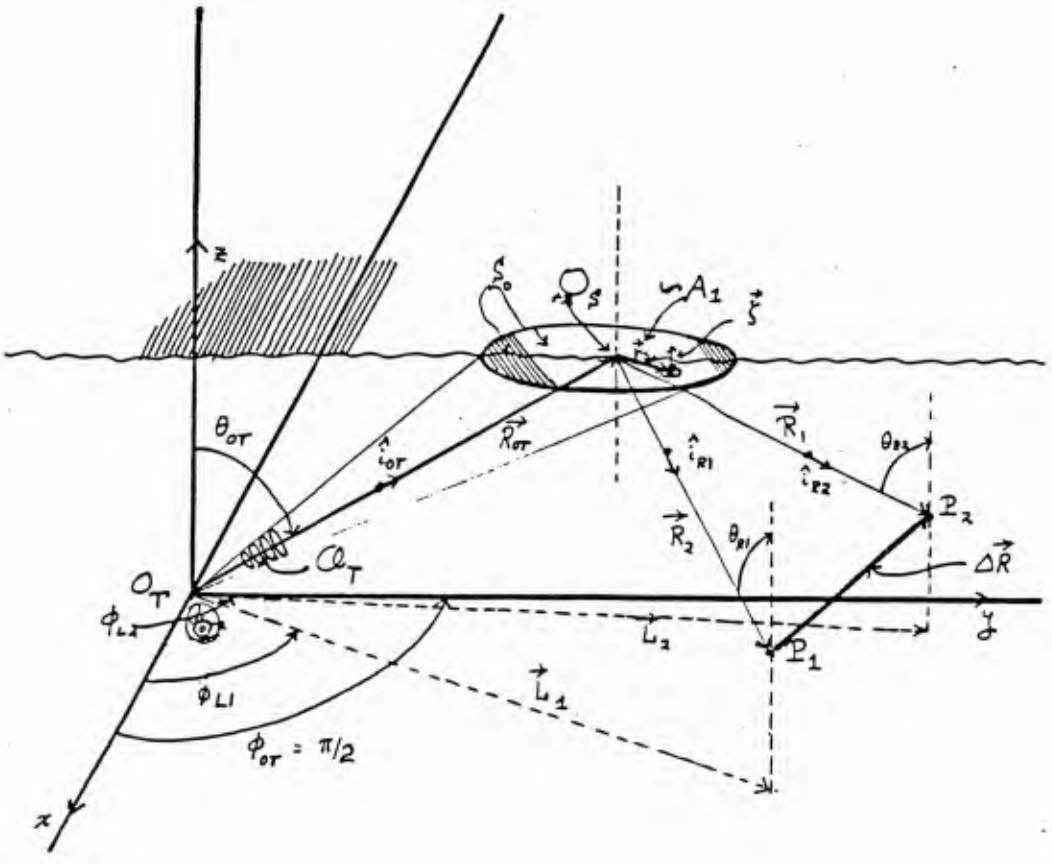

Figure 5.1. Geometry of the surface scattered field, observed at two points $P(\underline{R}_1)$, $P(\underline{R}_2)$, here in the far-field forward oblique scatter régime (ϕ_{L1}, $\phi_{L2} \neq \pi/2$; $\phi_{OT} = \pi/2$) with narrow transmitting beam A_1.

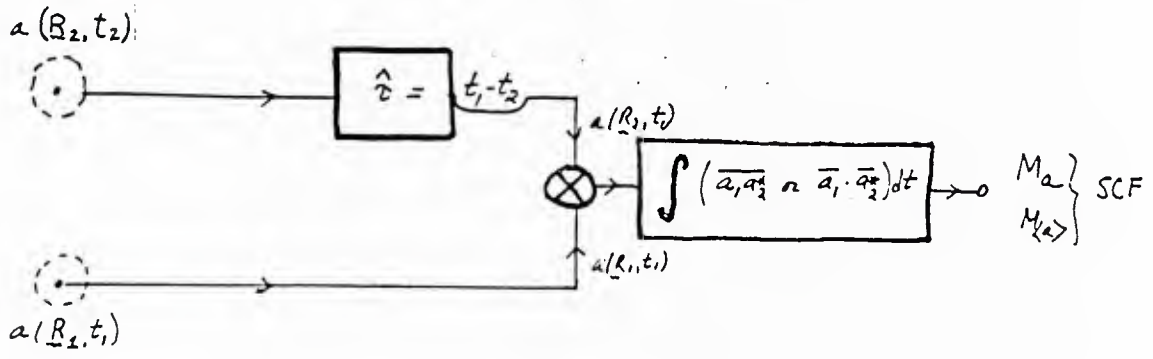

Figure 5.2. Cross-correlation scheme for measuring the Surface Coherence Functions (SCF), M_a, $M_{\langle a \rangle}$, Eq. (5.1).

5.1 PRELIMINARIES: FORMULATION

To obtain the desired SCF's, (5.1), we use in detail the analytical development of Part II Secs. 5-8, of [1], noting now the following:

(1) $R_{oR} \to R_1$ or R_2; $\quad \therefore \hat{\underline{i}}_{oR} \to \hat{\underline{i}}_{R1,2} = \underline{R}_{1,2}/|\underline{R}_{1,2}|$; (5.3a)

(2) $\underline{L}_o \to \underline{L}_1$ or $\underline{L}_2$, cf. Fig. 5.1; (5.3b)

(3) $2\underline{\alpha}_o \to 2\underline{\alpha}_{1,2}$, where (5.3c)

$$2\underline{\alpha}_{1,2} \equiv \left(\hat{\underline{i}}_{oT} - \hat{\underline{i}}_R\right)_{1,2} = \left\{ \hat{\underline{i}}_x \left[\left(1 + \frac{R_{oT}}{R}\right) \cos\phi_{oT} \sin\theta_{oT} - \frac{L}{R} \cos\phi_L \right] + \hat{\underline{i}}_y \left[\left(1 + \frac{R_{oT}}{R}\right) \sin\phi_{oT} \sin\theta_{oT} - \frac{L}{R} \sin\phi_L \right] + \hat{\underline{i}}_z \left(\cos\theta_{oT} + \cos\theta_R\right) \right\}_{1,2} \tag{5.3d}$$

$$= \left[\hat{\underline{i}}_x 2\alpha_x + \hat{\underline{i}}_y 2\alpha_y + \hat{\underline{i}}_z 2\alpha_z \right]_{1,2}$$

(4) $(2\alpha_z)_{1,2} \equiv b_{1,2}$ (5.3e)

(5) $c_o T_o \to (R_{oT} + R)$ (5-3f)

(6) $a_R = g_R = 1$; $a_{RT} \to a_T$. (5.3g)

Furthermore, for the general oblique scatter situation ($\phi_{L1 \text{ or } 2} \neq \pi/2$), the tilt-factors (3.3a,b) become

$$N^{(o)}_{\text{Gc-inc}} \to N^{(12)}_{\text{Gc-inc}} \doteq 16\alpha_{1z}\alpha_{2z} \left(\alpha_{1y}\alpha_{2y}\sigma^2_{Gy} + a_{1x}\alpha_{2x}\sigma^2_{Gx} + \alpha_{1z}\alpha_{2z}\right) \tag{5.4a}$$

$$N^{(o)}_{\text{GS-inc}} \to N^{(12)}_{\text{GS-inc}} \doteq 16 \Big\{ 3\alpha^2_{1x}\alpha^2_{2x}\sigma^4_{Gx} + 3\alpha^2_{1y}\alpha^2_{2y}\sigma^4_{Gy} + \left[(\alpha_{1y}\alpha_{2y} + \alpha_{2y}\alpha_{1z})^2 + 2\alpha_{1y}\alpha_{2y}\alpha_{1z}\alpha_{2z}\right]\sigma^2_{Gy} + \left[\alpha_{1x}\alpha_{2z} + \alpha_{2x}\alpha_{1z})^2 + 2\alpha_{1x}\alpha_{2x}\alpha_{1y}\alpha_{2z}\right]\sigma^2_{Gy} + \alpha^2_{1z}\alpha^2_{2z} \Big\} . \tag{5.4b}$$

Some simplification occurs for "forward" scatter régimes, where $\phi_{oT} = \phi_{L2} = \pi/2$, $\phi_{L2} \neq \pi/2$ say, cf. Fig. 5.1, as then $\alpha_{1x} = 0$ ($\neq \alpha_{2x}$), when used in (5.4a,b).*

With the above modifications, the acoustic field at $P(\underset{\sim}{R})$ is, again on neglecting diffraction effects,

$$a(\underset{\sim}{R},t) \doteq A_o \int_{Br_1} S_{in}(s/2\pi i) F_s^{(o)}(s|\zeta(\underset{\sim}{r},t),\ldots|f_o) e^{st} \frac{ds}{2\pi i},$$

where Br_1 is a Bromwich contour, cf. footnote p. 49, [1], while $A_o S_{in}(s/2\pi i)$ is the amplitude spectrum of the driving signal $S_{in}(t) = A_o s(t)$, $\langle s(t)^2 \rangle = 1$, $\langle S_{in}^2 \rangle = A_o^2/2$, with A_o the peak amplitude, vide Secs. 5.2, 5.3, [1]; (a_o = absorption coefficient, cf. (5.18), [1].) The quantity $F_S^{(o)}$ is here the appropriate TSSF (Total Surface Spreading Function) (7.7) of [1], from which the various desired second-order results, cf. (5.1), are constructed. This TSSF is explicitly now

$$\text{TSSF:}\quad F_S^{(o)} \doteq \frac{e^{-a_o\omega_o^2 (R_{oT}+R)}}{(4\pi)^2 R_{oT}^2 R^2} \int_{S_o} \left(\frac{s}{c_o}\right) \left[R_o S \frac{\hat{n} \cdot \underset{\sim}{\alpha}(\underset{\sim}{R})}{n_z}\right]_{G+S} a_T \cdot e^{-\frac{s}{c_o}\left[(\underset{\sim}{r}+\underset{\sim}{r}')\cdot \underset{\sim}{\alpha}(\underset{\sim}{R}) + R_{oT} + R\right]} dx\, dy, \tag{5.6}$$

where a_T is, as before, the (complex) beam pattern of the transmitter. With (5.5) and (5.6) we can proceed to construct M_a, $M_{\langle a \rangle}$, (5.1), using Sections 6 through 8 of [1], appropriately modified according to (5.3), (5.4) above.

---

*We note that our results (5.4a,b) above, and those following which involve second-order statistics, must be symmetrical in the indexes 1,2, since their designation is arbitrary.

5.2 THE SCF: COHERENT AND INCOHERENT SCATTER

For the various moments involved in (5.1), e.g., $\overline{a_1 a_2^*}$, $\overline{a_1}\cdot\overline{a_2}^*$, the exponentials resulting from (5.6) become

$$e^{-ik_o[(\underline{r}_1 + \underline{\zeta}_1)\cdot 2\underline{\alpha}_1 + (R_{oT} + R_1)]} \cdot e^{ik_o[(\underline{r}_1 + \underline{\Delta r} + \underline{\zeta}_2)\cdot 2\underline{\alpha}_2 + R_{oT} + R_2]} \tag{5.7}$$

$$= \exp\,[ik_o(2\underline{\alpha}_2\cdot\underline{\zeta}_2 - 2\underline{\alpha}_1\underline{\zeta}_1)]\,\exp\,[2ik_o\underline{\Delta\alpha}\cdot\underline{r}_1 + ik_o 2\underline{\alpha}_2\cdot\underline{\Delta r}]\,\exp ik_o\Delta R,$$

where $\underline{r}_2 = \underline{r}_1 + \underline{\Delta r}$ and

$$\Delta R \equiv R_2 - R_1; \quad \underline{\Delta\alpha} \equiv \underline{\alpha}_2 - \underline{\alpha}_1; \quad \underline{\alpha}_1 = \underline{\alpha}(R_1, \text{ etc.}), \text{ cf. (5.3d)};$$
$$\underline{\zeta}_1 = \underline{\zeta}(\underline{r}_1, t_1), \text{ etc.} \tag{5.7a}$$

A. The Coherent SCF

Next, from (7.13), [1] we consider the coherent SCF:

$$M_{\langle\alpha\rangle}^{(12)}(0) = \mathrm{Re}\left\{\hat{G}^{(1)}\hat{G}^{(2)} k_o^2 K_{in}(0) M_T^{(12)}(\infty|\ldots)\right\};\ \hat{G}^{(1),(2)} \equiv e^{-\rho_o\omega_o^2(R_{oT}+R_{1,2})} \tag{5.8}$$

where specifically

$$M_T^{(12)}(\infty|\ldots) = (2\alpha_{12})(2\alpha_{12}^*)\, A_T^{(12)}(\underline{\alpha})\left\langle e^{-2ik_o\alpha_{12}^* r}\right\rangle_f \left\langle e^{2ik_o\alpha_{12} r}\right\rangle_f \tag{5.8a}$$

$$A_T^{(12)} = \bar{R}_o^2\bar{S}^2 e^{ik_o\Delta R}\iint_{\underline{r}_1,\,d(\underline{\Delta r})} a_T(\underline{r}_1)\, a_T(\underline{r}_1+\underline{\Delta r})^* e^{2ik_o\underline{\Delta\alpha}\cdot\underline{r}_1 + 2ik_o\underline{\alpha}_2\cdot\underline{\Delta r}} \tag{5.8b}$$

$$= \bar{R}_o^2\bar{S}^2 e^{ik_o\Delta R}\, I_1(\underline{\alpha}_1, \underline{\alpha}_2). \tag{5.8c}$$

The integral I_1 is evaluated in Appendix A.2 for the basic Gaussian beam pattern [used in Sections 3 and 4 for a combined T and R pattern, cf. Secs. (6.3), (6.5) [1]:

$$a_T = g_T e^{-\frac{1}{2}\underline{r}\cdot\hat{\underline{C}}\cdot\underline{r}};\ \hat{\underline{C}} = \begin{bmatrix} A & 0 \\ 0 & B \end{bmatrix};\ \underline{r} = \hat{\underline{i}}_x x + \hat{\underline{i}}_y y, \tag{5.9}$$

where A, B are obtained here from (3.4a) on setting $A_R = 0$ therein, with $g_R = 1$; g_T, g_R are the beam gain factors, cf. 6.31 [1]. (Note that we have: (i) absorbed the k_o^2 into A and B, cf. (6.53) [1], which accordingly have the dimensions $[L^{-2}]$; and (ii), we have dropped the (complex) phase term in (5.9), as this is usually ignorable in these far-field cases.) The result for $A_T^{(12)}$ is

$$A_T^{(12)} = \bar{R}_o^2 \bar{S}^2 g_T^2 e^{ik_o\Delta R}\left(\frac{4\pi^2}{AB}\right) e^{-\frac{k_o^2}{2}\left[2\underline{\alpha}_1\cdot\hat{\underline{C}}^{-1}\cdot 2\underline{\alpha}_1 + 2\underline{\alpha}_2\cdot\hat{\underline{C}}^{-1}\cdot 2\underline{\alpha}_2\right]} \tag{5.10}$$

with

$$2\underline{\alpha}\cdot\hat{\underline{C}}^{-1}\cdot 2\underline{\alpha} = \frac{(2\alpha_x)^2}{A} + \frac{(2\alpha_y)^2}{B} \quad ; \quad \underline{\alpha} \Rightarrow \underline{\alpha}_\perp = \hat{\imath}_x\alpha_x + \hat{\imath}_y\alpha_y \tag{5.10a}$$

$$\text{and} \quad (2\pi)^2/AB = A_1^2, \ (3.4a). \tag{5.10b}$$

The coherent SCF (5.8) now becomes, with the help of (5.10) in (5.8a), in (5.8),

$$M_{\langle a\rangle}^{(12)}(\Delta R; R_1, R_2) = \frac{\bar{R}_o^2 \bar{S}^2 A_1^2 k_o^2 g_T^2 K_{in}(0)}{(4\pi)^4 R_{oT}^2 R_1 R_2} e^{-\alpha_o\omega_o^2(2R_{oT}+R_1+R_2)} \cdot e^{-(R_{g1}+R_{g2})/2}\cos k_o\Delta R \cdot e^{-\frac{k_o^2}{2}\left[2\underline{\alpha}_1\cdot\hat{\underline{C}}^{-1}\cdot 2\underline{\alpha}_1 + 2\underline{\alpha}_2\cdot\hat{\underline{C}}^{-1}\cdot 2\underline{\alpha}_2\right]} \tag{5.11}$$

where $R_{g1} = \sigma_G^2(2\alpha_{1z})^2 k_o^2$, $\sigma_G^2 = \overline{\zeta^2}$, cf. (3.4) et seq., is the Rayleigh number for $P(\underline{R}_1)$. As a check on (5.11), we see that it must reduce to (8.7), [1] when $R_2 \to R_1 \to R_{oR}$, $\therefore \underline{\alpha}_1 = \underline{\alpha}_2 = \underline{\alpha}_o$. This it does (when we correct (8.7): 3/4→1 in the exponent and 2 is removed in the denominator. Also, $b_{TRx} = b_{TRy} \doteq 0$ here, and $k_o^2\sigma_S^2 N(0)_{coh} \ll 1$ and is dropped; $g_R = 1 \to g_R$ again, etc.). Equation (5.11) holds for all frequencies and angles, subject to the conditions again of Appendix A.1, E,F.

B. The High Frequency Incoherent SCF

From Eqs. 7.34-7.35 of [1], and (7.11c), we can write the incoherent SCF, (5.1a), as

$$M_a^{(12)}(\tau=0)_{inc} = \mathrm{Re}\left\{k_o^2 \hat{G}^{(1)}\hat{G}^{(2)} K_o(0)_{in} M_T^{(12)}(0|\ldots)\right\}, \tag{5.12}$$

where in the high frequency cases Eq. (7.34a), [1], is extended to

$$\begin{aligned} M_T^{(12)}(0)_{hi\text{-}freq:\,A k_o^2 >> 1} \doteq \overline{R_o^2}\,\overline{S^2}\, e^{i k_o \Delta R}\Big\{ & A_{1\alpha} A_{2\alpha} \iint a_T(\underline{r}_1)\, a_T(\underline{r}_1+\underline{\Delta r})^* e^{2 i k_o \underline{\alpha}_2 \cdot \underline{\Delta r}} \\ & \cdot e^{2 i k_o \underline{\Delta\alpha}\cdot \underline{r}_1} F_2(-2\alpha_{1z} k_o, 2\alpha_{2z} k_o | 0)_G \, d\underline{r}_1 \, d(\underline{\Delta r}) \\ & + k_o^2 N_{GS\text{-}inc}^{(12)} \iint a_T(\underline{r}_1)\, a_T(\underline{r}_1+\underline{\Delta r})^* e^{2 i k_o \underline{\alpha}_2 \cdot \underline{\Delta r} + 2 i k_o \underline{\Delta\alpha}\cdot \underline{r}_1} \\ & \cdot K_S(\underline{\Delta r}, 0)\, d\underline{r}_1 \, d(\underline{\Delta r})\Big\}, \end{aligned} \tag{5.13}$$

in which now

$$A_{1\alpha,2\alpha} \equiv \left(\frac{\alpha_x^2 + \alpha_y^2 + \alpha_z^2}{\alpha_z/2} \right)_{1,2}, \tag{5.13a}$$

and $N_{GS\text{-}inc}^{(12)}$ is seen to be (5.4b) when $\phi_{oT} = \pi/2$, cf. Fig. 5.1.

Moreover, F_{2G} here becomes

$$F_2(-2\alpha_{1z} k_o, 2\alpha_{2z} k_o | 0) = e^{-\frac{1}{2} k_o^2 \sigma_G^2 [b_1^2 + b_2^2 - 2 b_1 b_2 \rho_G(\underline{\Delta r}, 0)]} \tag{5.14a}$$

$$\doteq e^{-\frac{1}{2} k_o^2 \underline{\Delta r}\cdot \underline{\hat{D}}_{12} \cdot \underline{\Delta r}}, \tag{5.14b}$$

from the high frequency expansion

$$\begin{aligned} \rho_G(\underline{\Delta r}, \tau) = 1 - \frac{1}{2!}\Big[& \sigma_{Gx}^2 (\Delta x)^2 + \sigma_{Gy}^2 (\Delta y)^2 + 2\Delta x \Delta y \frac{\rho_{G\text{-}xy}^2}{\sigma_G^2} + \tau \frac{\sigma_{\dot{r}}^2}{\sigma_G^2} - \tau \Delta x\, \sigma_{\dot{x}r}^2 \Big] \\ & + O(\Delta x^3, \tau^3), \end{aligned} \tag{5.14a}$$

where

$$\left.\begin{aligned}
\sigma_{Gx,y}^2 &\equiv \int_0^\infty K_G^2 \begin{matrix}\langle\cos^2\alpha\rangle \\ \langle\sin^2\alpha\rangle\end{matrix} \mathcal{W}_{G=g}(f_s)\,df_s, \quad \text{cf. (3.7)} - (3.12) \\
\sigma_{G\cdot xt}^2 &\equiv \int_0^\infty \omega_s K_G \overline{\cos\alpha}\, \mathcal{W}_{G=g}(f_s)\,df_s \quad ; \quad \sigma_G^2 = \langle j^2\rangle;\ \sigma_j^2 = \langle j^2\rangle; \\
\rho_{G\cdot xy}^2 &\equiv \int_0^\infty K_G^2 \langle\cos\alpha\,\sin\alpha\rangle \mathcal{W}_{G=g}(f_s)\,df_s
\end{aligned}\right\}. \qquad (5.14b)$$

Thus, the dyadic (or matrix) $\hat{\underline{D}}_{12}$ is

$$\hat{\underline{D}}_{12} = \begin{bmatrix} b_1 b_2 \sigma_{Gx}^2 & b_1 b_2 \rho_{G\cdot xy}^2 \\ b_1 b_2 \rho_{G\cdot xy} & b_1 b_2 \sigma_{Gy}^2 \end{bmatrix} = b_1 b_2 \begin{bmatrix} \sigma_{Gx}^2 & \rho_{G\cdot xy}^2 \\ \rho_{G\cdot xy}^2 & \sigma_{Gy}^2 \end{bmatrix} \doteq b_1 b_2 \begin{bmatrix} \sigma_{Gx}^2 & 0 \\ 0 & \sigma_{Gy}^2 \end{bmatrix}, \qquad (5.15)$$

where $\rho^2_{G\text{-}xy} \ll \sigma^2_{G\text{-}x,y}$ and

$$\hat{\underline{D}}_{12}^{-1} \doteq \frac{1}{b_1 b_2} \begin{bmatrix} \sigma_{Gx}^{-2} & 0 \\ 0 & \sigma_{Gy}^{-2} \end{bmatrix}; \quad \det \hat{\underline{D}}_{12} = b_1^2 b_2^2 \left(\sigma_{Gx}^2 \sigma_{Gy}^2 - \rho_{xy}^4\right) > 0. \qquad (5.15a)$$

Evaluating the integrals in (5.13) with the help of Appendix A.2 allows us to write

$$\boxed{\begin{aligned} M_T^{(12)}(0)_{k_0^2 A_j \gg 1} \doteq \overline{R_0^2}\,\overline{S^2}\, e^{\,i k_0 \Delta R} \Big\{ & A_{1\alpha} A_{2\alpha} I_2(\underline{\Delta\alpha}; \underline{\alpha}_1 + \underline{\alpha}_2)\, e^{-\frac{1}{2}\sigma_G^2 k_0^2 (b_1 - b_2)^2} \\ & + k_0^2 N_{GS'\text{-}mic}^{(12)} \int I_3(\underline{\Delta r}, \underline{\Delta\alpha})\, e^{2i k_0 \underline{\alpha}_1 \cdot \underline{\Delta r}} K_{S'}(\underline{\Delta r}, 0)\, d(\underline{\Delta r}) \Big\}, \end{aligned}} \qquad (5.16)$$

where, using (5.9) we get specifically ($\hat{\underline{D}}_{12} \gg \hat{\underline{C}}/2k_0^2$):

$$\underline{\text{(A.2-9)}}: \qquad I_2(\underline{\Delta\alpha}; \underline{\alpha}_1 + \underline{\alpha}_2) \doteq \frac{2\pi^2 g_T^2}{k_0^2 \sqrt{AB}\; b_1 b_2 \sigma_{Gx} \sigma_{Gy}} \cdot e^{-k_0^2 \underline{\Delta\alpha} \cdot \hat{\underline{C}}^{-1} \cdot \underline{\Delta\alpha}} \cdot e^{-\frac{1}{2}(\underline{\alpha}_1 + \underline{\alpha}_2) \cdot \hat{\underline{D}}_{12}^{-1} \cdot (\underline{\alpha}_1 + \underline{\alpha}_2)}, \qquad (5.17a)$$

$$\therefore\quad I_2(0;\underline{\alpha}_1+\underline{\alpha}_2=2\underline{\alpha}_0) \doteq \frac{2\pi^2 q_T^2}{k_0^2\sqrt{AB}\;b_0^2\sigma_{Gx}\sigma_{Gy}}\, e^{-\frac{1}{2}\left[\frac{(2\alpha_{0x})^2}{b_0^2\sigma_{Gx}^2}+\frac{(2\alpha_{0y})^2}{b_0^2\sigma_{Gy}^2}\right]} \qquad (5.17b)$$

$$b_1 = b_2 \to b_0 = 2\alpha_{0z}.$$

(A.2-6): $$I_3(\Delta\underline{r},\Delta\underline{\alpha}) = \frac{\pi q_T^2}{\sqrt{AB}}\, e^{-k_0^2\Delta\underline{\alpha}\cdot\hat{\underline{C}}^{-1}\cdot\Delta\underline{\alpha}}\left\{e^{-\frac{1}{4}\Delta\underline{r}\cdot\hat{\underline{C}}\cdot\Delta\underline{r}-ik_0\Delta\underline{\alpha}\cdot\Delta\underline{r}}\right\}, \qquad (5.18)$$

with

$$\Delta\underline{\alpha}\cdot\hat{\underline{C}}^{-1}\cdot\Delta\underline{\alpha} = \frac{(\alpha_{2x}-\alpha_{1x})^2}{A}+\frac{(\alpha_{2y}-\alpha_{1y})^2}{B}. \qquad (5.18a)$$

(A.2-8): $$I_1(\Delta\underline{\alpha};\underline{\alpha}_1+\underline{\alpha}_2) = I_2\Big|_{\hat{D}_{12}=0} = \frac{(2\pi)^2 q_T^2}{AB}\, e^{-k_0^2\Delta\underline{\alpha}\cdot\hat{\underline{C}}^{-1}\cdot\Delta\underline{\alpha}-k_0^2(\underline{\alpha}_1+\underline{\alpha}_2)\cdot\hat{\underline{C}}^{-1}\cdot(\underline{\alpha}_1+\underline{\alpha}_2)} \qquad (5.19)$$

$$= \frac{(2\pi)^2 q_T^2}{AB}\, e^{-2k_0^2\left[\underline{\alpha}_1\cdot\hat{\underline{C}}^{-1}\cdot\underline{\alpha}_1+\underline{\alpha}_2\cdot\hat{\underline{C}}^{-1}\cdot\underline{\alpha}_2\right]} \qquad (5.19a)$$

, cf. (5.10).

Noting once more that the correlation distance ℓ_S of the soliton layer is such that

$$\ell_S^2 \gg \frac{1}{4}\Delta\underline{r}\cdot\hat{\underline{C}}\cdot\Delta\underline{r} = \frac{A(\Delta x)^2}{4}+\frac{B(\Delta y)^2}{4}, \qquad (5.20)$$

since A, B are small, we see that $K_S(\Delta\underline{r},0)$ becomes small while $\Delta\underline{r}\cdot\hat{\underline{C}}\cdot\Delta\underline{r}/4$ itself remains near zero for values of $\Delta\underline{r}$ such that $K_S(\Delta\underline{r},o)\to 0$. Then we can set $\Delta\underline{r}\cdot\hat{\underline{C}}\cdot\Delta\underline{r}/4 \doteq 0$ in I_3, (5.18), and using I_2, (5.17a), obtain finally from (5.16) in (5.12) the desired high frequency generalization of (8.29),[1]:

$$M_a^{(12)}(\Delta R,R_1,R_2)\Big|_{\substack{inc\\ hi\,freq}} = \overline{R_o^2}\,\overline{S^2}A_1 q_T^2\frac{e^{-a_0\omega_0^2(2R_{oT}+R_1+R_2)}}{(4\pi)^4 R_{oT}^2 R_1 R_2}\,K_{in}(0)\cos k_0\Delta R$$
$$\cdot e^{-k_0^2\Delta\underline{\alpha}\cdot\hat{\underline{C}}^{-1}\cdot\Delta\underline{\alpha}}\left[\frac{A_{1\alpha}A_{2\alpha}\pi e^{-\frac{k_0^2}{2}\sigma_G^2(b_1-b_2)^2-(\underline{\alpha}_1+\underline{\alpha}_2)\cdot\hat{\underline{D}}^{-1}\cdot(\underline{\alpha}_1+\underline{\alpha}_2)/2}}{b_1 b_2\sigma_{Gx}\sigma_{Gy}}\right. \qquad (5.21)$$
$$\left.+\frac{k_0^4}{2}N_{Gc\text{-}inc}^{(12)}W_C\left[(\underline{\alpha}_1+\underline{\alpha}_2)_\perp k_0|0\right]+\frac{k_0^4}{2}N_{GS\text{-}inc}^{(12)}W_S\left[(\underline{\alpha}_1+\underline{\alpha}_2)_\perp k_0|0\right]\right],$$

with $\alpha_\perp = \hat{i}_x\alpha_x + \hat{i}_y\alpha_y$. Here we have added in the capillary component for completion, although it is always small vis-à-vis that of the soliton layer, provided, of course, that $\bar{U}_\infty > O(3\text{-}5$ m/sec), [4], [6a]. Equation (5.21) is discussed briefly in Sec. 5.4, along with the corresponding normalized SCF (= NSCF) developed in Sec. 5.3 below.

C. The Low-Frequency Incoherent SCF

Again, we follow the approach leading to (5.13), but now we use a direct expansion of F_{2G}, which leads to

$$M_T^{(12)}(0)\Big|_{\substack{inc\\low\text{-}freq}} \doteq \Big\{ e^{-k_o^2\sigma_G^2(b_1^2+b_2^2)/2}\left(\bar{R}_o^2\bar{S}^2 - \bar{R}_o^2\bar{S}^2\right)I_1 + \bar{R}_o^2\bar{S}^2\Big[k_o^2(b_1b_2)^2 \cdot \int I_3(\underline{\Delta r},\underline{\Delta\alpha})\, e^{2ik_o\underline{\alpha}_2\cdot\underline{\Delta r}} K_G(\underline{\Delta r},0)\, d(\underline{\Delta r}) + k_o^2 N_{GS\text{-}inc}^{(12)} \int I_3(\underline{\Delta r},\underline{\Delta\alpha})\, e^{2ik_o\underline{\alpha}_2\cdot\underline{\Delta r}} K_S(\underline{\Delta r},0)\, d(\underline{\Delta r})\Big]\Big\}. \tag{5.22}$$

Applying this to (5.12) yields finally

$$M^{(12)}(\Delta R,R_1,R_2)\Big|_{\substack{inc\\low\text{-}freq}} \doteq \bar{R}_o^2\bar{S}^2\hat{G}^{(1)}\hat{G}^{(2)}\frac{A_\perp}{2}g_T^2K_{in}(0)\cos k_o\Delta R\; k_o^4 e^{-k_o^2\underline{\Delta\alpha}\cdot\underline{\hat{C}}^{-1}\cdot\underline{\Delta\alpha}} \cdot\Big[(b_1b_2)^2W_g\left[k_o(\underline{\alpha}_1+\underline{\alpha}_2)_\perp|0\right] + N_{Gc\text{-}inc}^{(12)}W_c\left[k_o(\underline{\alpha}_1+\underline{\alpha}_2)_\perp|0\right] + N_{GS\text{-}inc}^{(12)}W_S\left[k_o(\underline{\alpha}_1+\underline{\alpha}_2)_\perp|0\right]\Big], \tag{5.23}$$

with $\hat{G}^{(1),(2)}$ given by (5.8), which is the desired generalization of (8.31), [1]. (We have neglected the first term in (5.22), since $\overline{R_o^2} \doteq \bar{R}_o$, $\overline{S^2} \doteq \bar{S}^2$, unless $\theta_{oT} > 85°$. We have also added the capillary component, as in (5.21), for completeness, although it is usually negligible vis-à-vis the soliton surface layer term.)

5.3 THE NORMALIZED SCF'S; EXTENSIONS

It is usually convenient to compare the SCF with its limiting form, which occurs when the two points of observation coincide, i.e., $R_1 \to R_2 \to R_{oR}$. Then $\underline{\alpha}_1 = \underline{\alpha}_2 = \underline{\alpha}_o$; $\underline{\Delta\alpha} = 0$, and the limiting form is, as expected, simply the

(unnormalized) scattering cross-section, or $M^{(0)}_{\langle a\rangle}(0)$, $M^{(0)}_{a-\langle a\rangle}(0)$, analogous to $M^{(0)}_{\langle X\rangle}(0)$, $M^{(0)}_{X-\langle X\rangle}(0)$ of [1], and Eqs. (A.1-1), (A.1-4) here. Accordingly, we define the normalized SCF (= NSCF) as follows, paralleling the definitions (2.10) and (2.6) [1], of coherent and incoherent Scattering Cross-Sections (SCS):

$$m^{(12)}_{coh} \equiv M^{(12)}_{\langle a\rangle} \cdot \left\{ \frac{R_1 R_2\ 4\pi\ (R_{oT} + R_1)\ 4\pi\ (R_{oT} + R_2)}{g_T^2\ A_{REF}\ K_{in}(0)\cdot(\text{path-loss})_1} \right\}, \tag{5.24}$$

$$m^{(12)}_{inc} \equiv M^{(12)}_{a} \cdot \left\{ \frac{R_1 R_2\ (4\pi R_{oT})^2}{g_T^2\ A_{REF}\ K_{in}(0)\cdot(\text{path-loss})_1} \right\}, \tag{5.25}$$

where the reference path loss is given by

$$(\text{path-loss})_1 \equiv e^{-2a_o\omega_o{}^2(R_{oT} + R_1)} \tag{5.26}$$

and, as before, $A_{REF} = A_1/2$, cf. (3.4a), and (A.1-5). Specific results for $m^{(12)}$ are then obtained from (5.11), (5.16), (5.23), in (5.24), (5.25). These results are presented and discussed in Section 2 preceding.

So far, we have focused on the SCF and NSCF for bi-static reception by unit gain ($g_R = 1$) omnidirectional (and $\therefore$ point) receivers. The beam projection parameters A, B, cf. (3.4a) and (5.9), are thus here

$$A = A_T/R_{oT}^2; \quad B = a_T^2(\theta_{oT})A_T/R_{oT}^2 . \tag{5.27}$$

However, we at once extend the present model to include receivers with general beam patterns: where g_T appears, write $g_T g_R$ and use (3.4a) for A and B, $A_R > 0$ now. (For a general discussion of beam patterns and surface projections, see Sec. 6 of [1].) The SCF and NSCF formally remain unchanged in these far-field cases: only C is modified to include the bounded receiving beam structure via A, B, (3.4a).

APPENDIX A.1: DEFINITIONS, ASSUMPTIONS, AND CONDITIONS

In this appendix we summarize a number of definitions, assumptions, and conditions which are directly pertinent to the analysis and results of this paper.

A. Incoherent Scattering Cross Sections, $\hat{\sigma}^{(o)}_{inc}$

Here we define

$$\hat{\sigma}^{(o)}_{inc} \equiv \frac{I^{(k=o)}_{incoh} \quad (\text{scattering at receiver R}) \cdot R^2_{oR}}{I_{incident}(\text{at surface})\, A_{REF}} [(\text{path loss}) \times (g_T g_R)^2]^{-1}, \tag{A.1-1}$$

where I_{incoh}, $I_{incident}$ are, respectively, the intensities of the scattered and incident fields at the points indicated. The basic concept of the scattering cross section (for surfaces) is to eliminate the effects of source level and propagation, i.e., the effects of the medium--which are handled separately--when computing energy loss, and to focus on the effects of the random scattering surface itself. For this reason, path loss (absorption), beam pattern gains (g_T, g_R), signal levels, and source and receiver distances are removed, where possible, as (A.1-1) indicates. To keep $\hat{\sigma}^{(o)}_{inc}$ dimensionless, a reference "illumination" area, A_{REF}, is employed, whose specific form is suggested by the composite beam pattern projection on the reference or equilibrium surface $\langle\zeta\rangle = 0$: S_o. Figure 3.1 shows the relevant geometry.

The various factors in Eq. (A.1-1) are given by

(A.1-2a) $I^{(k=o)}_{incoh}$ (scat. at receiver) = $M^{(o)}_{X-\langle X\rangle}(0)$ = intensity of the (incoherent) scattered field at the receiver (R), cf. Sec. 7.2 et seq.; Sec. 8 ff.; of [1].

(A.1-2b) $I_{incident}(\text{at surface}) = K_o(0)_{in}/(4\pi R_{oT})^2$ = intensity of the incident field at O_S, on the equilibrium scattering surface S_o;

(A.1-2c) g_T, g_R = the aperture "gain" of the transmitting and receiving systems, cf. (6.3), (6.7) of [1].

(A.1-2d) A_{REF} = a reference area on the equilibrium surface S_o, cf. Fig. 3.1, projected by the composite T and R beam patterns. (See C ff.).

(A.1-2e) "path loss" = $e^{-2a_o\omega_o^2 c_o T_o}$; $c_o T_o = R_{oT} + R_{oR}$; cf. Sec. 5.3, Eq. (5.18),[1]; (absorption)
ω_o ($=2\pi f_o$) is the (angular) frequency of the emitted signal; a_o is an absorption coefficient; c_o = (mean) wave front speed of sound in the water medium.

(A.1.2f) R_{oR} = distance of the receiver (origin) from O_S, Fig. 3.1.

(A.1.2g) R_{oT} = distance of the transmitter (origin) from O_S, Fig. 3.1.

(A.1.2h) $\underset{\sim}{\zeta}(\underset{\sim}{r},t)$ = (vector) wave surface elevation.

B. Coherent Scattering Cross Sections, $\hat{\sigma}^{(o)}_{coh}$

The coherent scattering cross section, $\hat{\sigma}^{(o)}_{coh}$, is formally the same as $\hat{\sigma}^{(o)}_{incoh}$, (A.1-1), except that now the incident intensity (2.7b) becomes

$$I_{incident(at\ the\ receiver)_{coh}} = K_o(0)_{in}/\{4\pi(R_{oT} + R_{oR})\}^2 \qquad (A.1\text{-}3)$$

which is the "mirror reflection" term. Thus, $I_{incid\text{-}coh} = (1/4)I_{incid\text{-}incoh}$, $R_{oT} = R_{oR}$, cf. (A.1-2b). In addition, $I^{(k=o)}_{incoh}$ is replaced by the coherent component $M^{(o)}_{\langle X\rangle}(0)$, cf. Sec. 7.2B, Eq. (8.7) [1]. Since only the "classical" or (k=0) component of the scattered field contains a potentially coherent contribution (excluding any direct field which may be received under certain mutual geometries), the complete coherent scatter cross section is now specifically

$$\hat{\sigma}^{(o)}_{coh} \equiv \frac{I^{(o)}_{coh}\ (\text{scattering at R})\ R^2_{oR}}{I_{incid}(\text{at the receiver R})\ A_{REF}}\ \{\text{path loss} \times (g_T g_R)2\}^{-1}, \qquad (A.1\text{-}4a)$$

or*

$$\hat{\sigma}^{(o)}_{coh} = \frac{R^2_{oR}\{4\pi(R_{oR} + R_{oT})\}^2\ M^{(o)}_{\langle X\rangle}(0)}{(g_T g_R)^2\ A_{REF}\ K_o(0)_{in} \cdot (\text{path loss})}\ . \qquad (A.1\text{-}4b)$$

The conventional, coherent definition usually employed is simply the "plane wave" coherent reflection coefficient*

$$\hat{R}_{coh} \equiv |\langle e^{2ik_o\alpha_o\zeta_G}\rangle| = e^{-R_g/2}, \quad R_g \equiv (2\alpha_{oz}\sigma_G k_o)^2. \qquad (A.1\text{-}4c)$$

C. The Reference Area, A_{REF}

The reference area A_{REF} appearing in the above definitions of the scattering cross sections, (2.6), (2.10), while arbitrary, depends on the beam pattern projections on S_o. From Section 6.5 IV, (6.56),[1], our choice of reference area is specifically

$$A_{REF} = \mathcal{A}_1/2, \quad \mathcal{A}_1 = 2\pi/\sqrt{AB(\theta_{oT})}, \qquad (A.1\text{-}5)$$

where $\mathcal{A}_1$ is the projected area (on S_o) of the combined gaussian-omnidirectional beam pattern used specifically in this study.

D. Some Definitions and Parameters

The various elements of (A.1-4), (3.1) are specifically:

$\overline{\mathcal{R}_o^2}$, $\overline{\mathcal{R}_o}$ = mean-square, mean, reflection coefficients (=1, for water-air interfaces);

$\overline{\mathcal{S}^2}$, $\overline{\mathcal{S}}$ = mean-square, mean, shadowing function, see Sec. 7.4C, [1];

σ^2_{Gx}, σ^2_{Gy} = $\langle\zeta^2_{Gx}\rangle$, $\langle\zeta^2_{Gy}\rangle$: ($\zeta_{Gx} = \frac{\partial\zeta_G}{\partial x}$, etc.): mean-square slopes of the gravity-capillary wave component, cf. Sec. 7.4B, [1];

*The formal conversion of $\hat{\sigma}_{coh}$ to the scattering coefficient R_{coh} currently used in the Navy's propagation loss programs is embodied in the relation $\hat{\sigma}_{coh} = F_o(\text{range, pathloss, etc.}) \cdot \hat{R}^2_{coh}$, where F_o is given explicitly by the coefficient of exp $(-R_g)$ in (3.4). See Eq. (6.44b) of [16]: $\mathcal{R}$ therein is set equal to unity here.

(A.1-6) cont'd

σ_c^2 = $\langle \zeta_c^2 \rangle$: mean-square height (about $\langle \zeta_c \rangle = 0$) of the "capillary" wave surface;

σ_S^2 = $\langle \zeta_S^2 \rangle$: mean-square height of the soliton "bumps";

W_c = surface wave number intensity spectrum of ζ_c with

$$\sigma_G^2 \hat{\rho}_c(\underset{\sim}{\Delta r}, 0) = \int_{\underset{\sim}{k}_D}^{\infty} W_c(\underset{\sim}{k}|0) \cos(\underset{\sim}{k} \cdot \underset{\sim}{\Delta r}) \frac{d\underset{\sim}{k}}{(2\pi)^2}, \text{ cf. (8.25), [1];}$$

W_S = wave number spectrum of the soliton-ripple

$$= \sigma_S^2 \hat{w}_S = \int_{-\infty}^{\infty} K_S(\underset{\sim}{\Delta r}|0) e^{i\underset{\sim}{k} \cdot \underset{\sim}{\Delta r}} \, d(\underset{\sim}{\Delta r})$$

and $\hat{w}_S = W_S/\sigma_S^2$ = normalized spectrum;

$\mathcal{A}_1$ = Eq. (A.1-5);

b_o = $\cos \theta_{oT} + \cos \theta_{oR}$.

The directional vector $2\alpha_o$ is (cf. Sec. 5.5, Fig. 5.1, [1], and (3.2) here

$$2\underset{\sim}{\alpha}_o = \hat{\underset{\sim}{\imath}}_{oT} - \hat{\underset{\sim}{\imath}}_{oR} = \hat{\underset{\sim}{\imath}}_x \left\{ (1 + \frac{R_{oT}}{R_{oR}}) \cos \phi_{oT} \sin \theta_{oT} - \frac{L_o \cos \phi_{oL}}{R_{oR}} \right\}$$

$$+ \hat{\underset{\sim}{\imath}}_y \left\{ (1 + \frac{R_{oT}}{R_{oR}}) \sin \phi_{oT} \sin \theta_{oT} - \frac{L_o \sin \phi_{oL}}{R_{oR}} \right\} + \hat{\underset{\sim}{\imath}}_z b_o \qquad \text{(A.1-7)}$$

for arbitrary angles of illumination and observation. [In all earlier applications, we have used $\phi_{oL} = \pi/2$: the z, y-axis form a plane containing O_T and O_R.]

Important special cases of (A.1-7) are:

(i) Backscatter (R@T): ($L_o = 0$; $\theta_{oR} = \theta_{oT}$; $\hat{\underset{\sim}{\imath}}_{oR} = -\hat{\underset{\sim}{\imath}}_{oT}$; $R_{oR} = R_{oT}$; $h_R = h_T$; $\phi_{oR} = \phi_{oT} + \pi/2$; cf. Fig. 2.2).

$$\therefore 2\underset{\sim}{\alpha}_o = 2(\hat{\underset{\sim}{\imath}}_x \cos \phi_{oT} \sin \theta_{oT} + \hat{\underset{\sim}{\imath}}_y \sin \phi_{oT} \sin \theta_{oT} + \hat{\underset{\sim}{\imath}}_z \cos \theta_{oT}); \qquad \text{(A.1-9a)}$$

$$(\alpha_{ox}^2 + \alpha_{oy}^2 + \alpha_{oz}^2)\ (\alpha_{oz}/2) = 2/\cos\theta_{oT}. \qquad \text{(A.1-9b)}$$

(ii) Bistatic at the Snell Angle ($R \neq T$); $L_o \neq 0$:

$$\left.\begin{aligned} &(\hat{\underline{i}}_{oR})_x = (\hat{\underline{i}}_{oT})_x \text{ when } \phi_{oT} = \pi/2 = (\phi_{oR} - \pi/2); \\ &(\hat{\underline{i}}_{oR})_y = (\hat{\underline{i}}_{oT})_y \text{ when } L_o = (R_{oT} + R_{oR}) \sin\theta_{oT}; \\ &(\hat{\underline{i}}_{oR})_z = -(\hat{\underline{i}}_{oT})_z \text{ when } \theta_{oR} = \theta_{oT}; \end{aligned}\right\} \text{Snell plane} \qquad \text{(A.1-8a)}$$

$$\therefore 2\underline{\alpha}_o = 2\hat{\underline{i}}_z \cos\theta_{oT}, \text{ or } \underline{\alpha}_o = \hat{\underline{i}}_z \cos\theta_{oT}; \qquad \text{(A.1-8b)}$$

$$(\alpha_{ox}^2 + \alpha_{oy}^2 + \alpha_{oz}^2)/(\alpha_{oz}/2) = 2\cos\theta_{oT}. \qquad \text{(A.1-8c)}$$

Otherwise, (A.1-7) is the general relation. Other generalizations are considered in Section 5.

E. Principal Assumptions and Approximations: (High Frequency Régimes):

The principal assumptions and approximations pertaining to our general high-frequency results are:

(A.1-9)
(1) Far-field (Fraunhofer) geometries, cf. Sec. 5.5, [1];
(2) Narrowband signals (so that we may treat time parametrically in the moving wave surface vis-à-vis the acoustic signal); cf. remarks after Eq. (5.21b), [1];
(3) Narrow beams (cf. Sec. 6.6), [1], at least one narrow beam;
(4) Neglects diffraction terms: $k \geq 1$: "Diffuse" scatter and multiple scatter (cf. Sec. 3.3; also Sec. 8.5 of [1]);
(5) Small Rayleigh numbers for the small scale surfaces, $\zeta_{c,S}$: $R_{c,S} \equiv (k_o b_o \sigma_{c,S})^2 << 1$;
(6) The capillary and soliton surfaces (ζ_c, ζ_S) are "small-scale," e.g., $\ell_{c,S} << \ell_g$: the correlation distance of the gravity-wave component is much larger than that of the capillary and soliton waves;

(7) The small-scale surfaces are statistically independent of the gravity wave surface component (vide remarks in Sec. 7.3A, Eq. (7.19) et seq. of [1]);

(8) Both components of the wave surface are essentially homogeneous and stationary, at least over the "illuminated" area and for times long compared to the duration of the incident signal.

A few words are appropriate here, to note the limitations of the Kirchoff or "tangent-plane" method used throughout our analysis (and vide [1], [2] also). The basic constraint for the Kirchoff method, which relates the curved character of the surface and the (mean) incident wavelength, λ_o, is expressed by the relations

$$2\pi\rho/\lambda_o >> 1, \text{ or more strictly, } (2\pi\rho/\lambda_o)^{1/3} >> 1, \qquad \text{(A.1-10)}$$

in which ρ is the (rms) radius of curvature of the wave surface. The first relation of (A.1-10) is a less strict version of the second, cf. Chapter 7 of [9]. Thus, for frequencies $f_o(=c_o/\lambda_o)$ much below O(1 kHz) we may expect difficulties in the applicability of the Kirchoff method: let f_o = 300 Hz, $\therefore \lambda_o$ = 5m, so that $2\pi\rho/5 >> 1$ or $(2\pi\rho/5)^{1/3} >> 1$ requires $\rho \geq$ O(5-10m), or O(30-40m), respectively. For composite surfaces, like those treated here where the effects of the "capillary" component of the gravity-capillary continuum may be neglected vis-à-vis those of the truly additional (here, soliton) layer, these conditions (A.1-10) are reasonably satisfied by the gravity-wave portions (g) of the underlying surface (G=g+c). Accordingly, we may expect that for f_o > O(100-200 Hz) the Kirchoff method can be used, with increasing confidence at the higher frequencies.

Below O(100-200 Hz) the method breaks down and alternative, perturbational approach must be employed, cf. Chapter 3 of [9]. The conditions of applicability here thus require

$$2\pi\sigma_G << \lambda_G \text{ and } 8\sigma_G \sin\psi << \lambda_o, \qquad \text{(A.1-11)}$$

where $\sigma_G^2 = \zeta^2 = \sigma^2$ and ψ = grazing angle, with ℓ_G = the surface correlation distance (radius), of the gravity-wave component. Moreover, the perturbational approach requires small (rms) slopes, e.g.,

$$\langle \nabla\zeta \cdot \nabla\zeta \rangle^{1/2} << 1, \qquad \text{(A.1-12)}$$

a condition not required in the tangent plane method. From (A.1-11), then, we may expect the perturbational approach to break down for "high" frequencies, e.g., f_o = O(1 kHz), and moderate (or stronger) sea states ($\overline{U_\infty}$ = 10 m/s), where $\sigma_{G=g}$ becomes 0.38 m. (3.23a). Thus, at $\psi = 10°$, $\sin\psi = 0.174$ and (A.1-11) requires that 0.53 m $<<$ λ_o, while f_o = 1 kHz λ_o = 1.5m.

To sum up, we should be wary of using the Kirchoff method here for frequencies below O(0.1-0.2 kHz), while the perturbational approach should not be used for f_o > O(1 kHz) in the present instances. Moreover, as already noted above and in [1], at small grazing angles ($\psi \leq 25°$) a small (additive) correction O(1.0 dB @ 25°) → O(2.5 dB @ 5°-10°) to the scattering cross-section $\hat{\sigma}^{(o)}$ is needed, to account for the increasing inaccuracies of the tangent plane approach as $\psi \to 0$; (see Fig. 13 of [18], and ref. 20 therein).

F. Additional Assumptions and Approximations

The approximations and assumptions governing (5.6) are:

(1) narrowband signals: these permit us to separate the signal components from the wave surface velocity $\dot{\zeta}$: the total surface spreading function $F_S^{(\ell)}(s', s-s')$ is ~ $\delta(s-s')$, to yield $F_S^{(\ell)}(s,t|..)$ in (5.6) and in (5.21a), (5.26) of [1].

(2) Small doppler:

(3) far-field conditions: $\pi L_{max}\ell_{max}/\lambda_o << R_{oT}, R_{oR}$, where ℓ_{max} = max (rms) correlation distance of the (illuminated) wave surface; L_{max} = maximum dimension of the transmitter (receiver) aperture. This permits us to define beam patterns, which are independent of range.

(4) small surface displacements: vis-à-vis R_{oT}, R_{oR}: (part of (3), really).

(5) "narrow beams," (N.B.): $\Delta S_o \ll R_{oT}^2, R_{oR}^2$: beam patterns are independent of angle variations and can be referred to a single point (O_S) on the "illuminated" wave surface. [If the "narrow-beam" condition is not satisfied, (5.21b) of [1] is to be used in place of (5.6).]

(6) $\nabla c = 0$: $c(z) = c_o$, a constant: no velocity gradients in the volume.

(7) $\hat{Q}_V = 0$: no volume inhomogeneities, random or deterministic, cf. Eq. (5.3b) of [1].

(8) Only local surface scatter interactions: the scattered field does not couple to the scattering elements, cf. (5.3c,d) et seq. of [1].

(9) $\hat{M}_\Sigma \to \hat{M}_\infty$: the scattering surface is sufficiently removed not to affect the pressure distribution over the aperture of the driving signal source, cf. (5.1) of [1]. (This condition is always obeyed in practice unless the boundary is very close to the aperture and the source level is very high, Ref. [41, I] of [1].

(10) A non-dispersive, lossy medium is assumed, so that the Helmholtz equation (5.3a), [1] for the propagating field is obeyed, with only a frequency and range-dependent attenuation factor applied to the emitted signal amplitude, A_o, cf. (5.8), in conjunction with (1) above. For practical oceans this requires $f_o \leq 0(40\ \text{kHz})$.

(11) Slowly moving surfaces vis-à-vis c_o and the time-scale of the injected signal: this permits us to treat the time-variability of $\zeta(\underset{\sim}{r},t')$ parametrically.

A.2 BEAM PATTERN INTEGRALS

In developing the results for the Surface Coherence Function (SCF), cf. Sec. 5 earlier, we encounter three important integrals which arise from the projection of the source (and sometimes receiving) beam patterns on the equilibrium wave surface, $\zeta = 0$. These are

$$I_3(\underset{\sim}{\Delta r}, \underset{\sim}{\Delta\alpha}) \equiv \int_{-\infty}^{\infty} \mathcal{A}_T(\underset{\sim}{r}_1)\mathcal{A}_\eta(\underset{\sim}{r}_1+\underset{\sim}{\Delta r})^* e^{2ik_o \underset{\sim}{\Delta\alpha}\cdot\underset{\sim}{r}_1} d\underset{\sim}{r}_1 \quad , \quad \underset{\sim}{\Delta\alpha} \equiv \underset{\sim}{\alpha}_2 - \underset{\sim}{\alpha}_1 \ ; \qquad \text{(A.2-1)}$$

$$I_2(\underline{\Delta\alpha}, \underline{\alpha}_1 + \underline{\alpha}_2) \equiv \int\int_{-\infty}^{\infty} a_T(\underline{r}_1) a_T(\underline{r}+\underline{\Delta r})^* \left\{ e^{2ik_0 \underline{\alpha}_2 \cdot \underline{\Delta r} - \frac{1}{2} k_0^2 \underline{\Delta r} \cdot \hat{\underline{D}}_{12} \cdot \underline{\Delta r}} \right\} e^{2ik_0 \underline{\Delta\alpha} \cdot \underline{r}_1} d(\underline{\Delta r}) \quad \text{(A.2-2)}$$

$$= \int_{-\infty}^{\infty} I_3(\underline{\Delta r}, \underline{\Delta\alpha}) e^{2ik_0 \underline{\alpha}_2 \cdot \underline{\Delta r} - \frac{k_0^2}{2} \underline{\Delta r} \cdot \hat{\underline{D}}_{12} \cdot \underline{\Delta r}} d(\underline{\Delta r}); \quad \text{(A.2-2a)}$$

and

$$I_1(\underline{\Delta\alpha}, \underline{\alpha}_1 + \underline{\alpha}_2) \equiv I_2 \Big|_{\hat{\underline{D}}_{12} = 0} = \int_{-\infty}^{\infty} I_3(\underline{\Delta r}, \underline{\Delta\alpha}) e^{2ik_0 \underline{\alpha}_2 \cdot \underline{\Delta r}} d(\underline{\Delta r}); \quad \underline{\Delta r} \equiv \underline{r}_1 - \underline{r}_2 . \quad \text{(A.2-3)}$$

Here the beam pattern projection a_T is given by

$$a_T = q_T e^{-\frac{1}{2} \underline{r} \cdot \hat{\underline{C}} \cdot \underline{r}} ; \quad \hat{\underline{C}} = \begin{bmatrix} A & 0 \\ 0 & B \end{bmatrix} ; \quad \underline{r} = \hat{\underline{i}}_x x + \hat{\underline{i}}_y y , \quad \text{(A.2-4)}$$

cf. (5.9), with $\det \hat{\underline{C}} = AB$, where $A, B \geq 0$ are given by (3.4a); see Sec. 6 of [1] for details. The integrals (A.2-1) to (A.2-3) are generalizations of (6.34) to (6.36) of [1].

We begin with I_3 and use the general result

$$I(\underline{\xi}) = \int_{[u]} e^{i \underline{\xi} \cdot \underline{u} - \frac{1}{2} \underline{u} \cdot \hat{\underline{A}} \cdot \underline{u}} \underline{du} = \frac{(2\pi)^{n/2}}{(\det \hat{\underline{A}})^{1/2}} e^{-\underline{\xi} \cdot \hat{\underline{A}}^{-1} \cdot \underline{\xi}/2} \quad \text{(A.2-5a)}$$

(in vector form, where $\hat{\underline{A}}$, $\hat{\underline{A}}^{-1}$ are dyadics), or equivalently

$$I(\underline{\xi}) = \int_{[u]} e^{i \tilde{\underline{\xi}} \underline{u} - \frac{1}{2} \tilde{\underline{\xi}} \hat{\underline{A}} \underline{\xi}} \underline{du} = \frac{(2\pi)^{n/2}}{(\det \hat{\underline{A}})^{1/2}} e^{-\tilde{\underline{\xi}} \hat{\underline{A}}^{-1} \underline{\xi}/2} \quad \text{(A.2-5b)}$$

in matrix form, where $\underline{\xi}$ is a vector, $\tilde{\underline{\xi}}$ its transpose, etc., $\hat{\underline{A}}$ = (n x n) matrix; n = dimension of the vectors; here n=2. Continuing with the help of (A.2-5) applied to (A.2-1) with (A.2-4) yields at once

$$\boxed{I_3(\underline{\Delta r}, \underline{\Delta\alpha}) = \frac{\pi q_T^2}{\sqrt{AB}} e^{-k_0^2 \underline{\Delta\alpha} \cdot \hat{\underline{C}}^{-1} \cdot \underline{\Delta\alpha}} \cdot e^{-\underline{\Delta r} \cdot \hat{\underline{C}} \cdot \underline{\Delta r}/4 - ik_0 \underline{\Delta\alpha} \cdot \underline{\Delta r}}} \quad \text{(A.2-6)}$$

Similarly, I_2, (A.2-2), becomes from (A.2-3) and (A.2-6)

$$I_2 = \frac{\pi q_T^2}{\sqrt{AB}} e^{-k_o^2 \underline{\Delta\alpha}\cdot\hat{\underline{C}}^{-1}\cdot\underline{\Delta\alpha}} \int_{-\infty}^{\infty} e^{-\frac{1}{2}\underline{\Delta r}\cdot(k_o^2\hat{\underline{D}}_{12}+\hat{\underline{C}}/2)\cdot\underline{\Delta r}} e^{i k_o(\underline{\alpha}_1+\underline{\alpha}_2)\cdot\underline{\Delta r}} d(\underline{\Delta r})$$

$$\therefore \boxed{I_2 = \frac{2\pi^2 q_T^2 e^{-k_o^2\underline{\Delta\alpha}\cdot\hat{\underline{C}}^{-1}\cdot\underline{\Delta\alpha}}}{k_o^2\left[\det\hat{\underline{C}}\,(\hat{\underline{D}}_{12}+\hat{\underline{C}}/2k_o^2)\right]^{1/2}} \cdot e^{-\frac{1}{2}(\underline{\alpha}_1+\underline{\alpha}_2)\cdot(\underline{D}_{12}+\hat{\underline{C}}/2k_o^2)^{-1}\cdot(\underline{\alpha}_1+\underline{\alpha}_2)}} \quad \text{(A.2-7)}$$

where we have used (A.2-5) once more.

Setting $\hat{\underline{D}}_{12} = 0$ in (A.2-7) gives us at once I_1, which is specifically now

$$\boxed{I_1(\underline{\alpha}_1,\underline{\alpha}_2) = \frac{(2\pi)^2 q_T^2}{AB} e^{-\frac{k_o^2}{2}\left[2\underline{\alpha}_1\cdot\hat{\underline{C}}^{-1}\cdot 2\underline{\alpha}_1 + 2\underline{\alpha}_2\cdot\hat{\underline{C}}^{-1}\cdot 2\underline{\alpha}_2\right]}} \quad \text{(A.2-8)}$$

where we have used $\Delta\underline{\alpha} = \underline{\alpha}_2 - \underline{\alpha}_1$. As expected in all of the above, these integrals are symmetrical in $\underline{\alpha}_1$ and $\underline{\alpha}_2$; ($\hat{\underline{C}}$, $\hat{\underline{D}}$ are symmetric matrices/dyadics). This symmetry follows from the arbitrary definitions of $P(\underline{R}_1)$ and $P(\underline{R}_2)$, as well as of R_1, R_2, etc.

Finally, we note that when $\hat{\underline{D}}_{12} >> \hat{\underline{C}}/2k_o^2$, (A.2-7) reduces to

$$I_2(\underline{\Delta\alpha}, \underline{\alpha}_1+\underline{\alpha}_2) = \frac{2\pi^2 q_T^2}{k_o^2\left[\mathrm{Det}\,\hat{\underline{C}}\,\hat{\underline{D}}_{12}\right]^{1/2}} e^{-k_o^2\underline{\Delta\alpha}\cdot\hat{\underline{C}}^{-1}\cdot\underline{\Delta\alpha}} \cdot e^{-\frac{1}{2}(\underline{\alpha}_1+\underline{\alpha}_2)\cdot\hat{\underline{D}}_{12}^{-1}\cdot(\underline{\alpha}_1+\underline{\alpha}_2)} \quad \text{(A.2-9)}$$

$$\hat{\underline{D}}_{12} >> \hat{\underline{C}}/2k_o^2 ,$$

which yields (5.17a).

REFERENCES

[1] D. Middleton, "Acoustic Scattering from Truly Composite Wind-Wave Surfaces: Scattering Without Bubbles," NUSC Technical Document TD-7205, 20 August 1984, NUSC, New London Laboratory, New London, CT 06320.

[2] _____, "Acoustic Scattering from Truly Composite Wind-Wave Surfaces II: Backscatter Cross Sections and Doppler Effects at High Frequencies and Small Angles for Bubble-Free Régimes," NUSC Technical Report TR-7635, 22 July 1986, NUSC, New London Laboratory, New London, CT 06320.

[3] D. Middleton and R. H. Mellen, "Wind-Generated Solitons: A Potentially Significant Mechanism in Ocean Surface Wave Generation and Surface Scattering," IEEE Journal of Oceanic Engineering, 10, No. 4, October 1985, pp. 471-476.

[4] D. Middleton, "A Proposed Soliton Mechanism in Wind-Wave Surface Generation and Scattering," NUSC Technical Report TR-7775, 19 December 1986, NUSC, New London Laboratory, New London, CT 06320.

[5] _____, "Acoustic Scattering by Wind-Generated Wave-Surface Solitons: A Critical Summary," First IMACS Symposium, Yale University (New Haven, CT), August 6-8 1986, published in Proceedings, First IMACS Symposium on Computational Acoustics, North Holland Publishing Company, Spring 1987.

[6] D. Middleton and R. H. Mellen, "A Proposed Surface Soliton Mechanism in Wind-Wave Generation and Scattering: Experimental Evidence and Preliminary Theory," submitted, JASA, February 1987.

[7] R. H. Mellen, D. Middleton, and J. W. Fitzgerald, "Sea Surface Backscattering and the Soliton Mechanism," NUSC Technical Document TD-7583, 21 February 1986, NUSC, New London Laboratory, New London, CT 06320.

[8] W. I. Roderick and J. B. Chester, R. K. Dullea, "High-Frequency Acoustic Backscatter from the Sea Surface," NUSC Technical Document TD-7183, 12 July 1984, NUSC, New London Laboratory, New London, CT 06320.

[9] F. G. Bass and I. M. Fuks, Wave Scattering from Statistically Rough Surfaces (Translated and edited by C. B. and J. F. Vesecky), Pergamon Press (New York), 1979.

[10] S. A. Kitaigorodskii, The Physics of Air-Sea Interaction [Transl. 1973 Israel Program for Scientific Translations, U.S. Department of Commerce, available NTIS, Springfield, VA 22151], Section 6.3.

[11] W. L. Pierson, Jr. and L. Moscowitz, "A Proposed Spectral Form for Fully-Developed Wind Seas Based on the Similarity Theory of S. A. Kitaigorodskii," J. Geophysics Research 69, 5180-5190, No. 24, 1964.

[12] O. M. Phillips, The Dynamics of the Upper Ocean, Cambridge University Press (New York), 1966; See Section 3.2.

[13] H. Mitsuyasu and T. Honda, "The High-Frequency Spectrum of Wind-Generated Waves," J. Oceanographic Soc. Japan 30, pp. 185-198, 1974.

[14] H. Mitsuyasu, "Measurement of the High-Frequency Spectrum of Ocean Wave Surfaces," J. Physical Oceanography 7, pp. 882-891, 1977.

[15] C. S. Cox and W. H. Munk, "Measurement of the Roughness of the Sea Surface from Photographs of the Sun's Glitter," J. Optical Soc. Amer., Volume 44, No. 11, pp. 838-850, 1954.

[16] I. Tolstoy and C. S. Clay, Ocean Acoustics: Theory and Experiment in Underwater Sound, McGraw-Hill (New York), 1966.

[17] D. Middleton, An Introduction to Statistical Communication Theory, McGraw-Hill (New York), 1960. Reprint Edition, Penninsula Publishing, P.O. Box 867, Los Altos, CA 94020, June 1987, Section 1.5.

[18] S. T. McDaniel and A. D. Gorman, "Examination of the Composite-Roughness Scattering Model," J. Acous. Soc. Amer. 73, No. 5, May 1983, pp. 1476-1486.

INITIAL DISTRIBUTION LIST

Addressee	No. of Copies
NAVSEASYSCOM (SEA-63D (CDR E. Graham))	1
NORDA (Code 113 (Dr. B. Adams); 243 (Dr. R. Love, Dr. R. Farwell); 245 (Dr. W. Kinney); 240 (Dr. T. Goldsberry); 331 (Dr. M. Y. Su))	6
NOSC (Code 013 (Dr. E. Cooper) (3); 7133 (Dr. C. Persons); 5322 (Dr. J. Northrup); (B. Smith); (Dr. F. Fisher, Dr. F. Spiess, Dr. V. Anderson (Marine Physical Labs))	8
SACLANTCTR (Tech. Director, Dr. R. Goodman; ATD, Dr. R. Martin)	2
ONR (Code 1125 AO (Dr. R. M. Fitzgerald); 1125 AR (G. Johnson, R. Obrochta); 1111 SP (J. Simpson, Dr. N. Gerr); 111 (B. Junker); 112 (G. Hamilton); 1122B (E. Hartwig); 1111 (Dr. Ringeisen))	10
NRL (Code 5160 (Dr. E. Franchi); 5303 (Dr. L. Wetzel))	2
ITS/NTIA (U.S. Dept. of Commerce (Dr. A. Spaulding, Dr. C. Rush))	2
ARL/UNIV OF TEXAS (Dr. G. Wilson, G. Ellis, Prof. C. Horton, Dr. H. Boehme, Dr. R. Culbertson)	5
DTIC	12
NAVPGSCOL (Prof. H. Medwin, (1) Library)	2
SAIC (W. Chadsey, Dr. R. Becherer, Dr. Tatrow, Dr. M. J. Brackett Hersey, Dr. R. Green)	5
YALE UNIVERSITY (Prof. P. H. Schultheiss)	1
Scripps Inst. of Oceanography, La Jolla, CA (Dr. W. Munk)	1
ARL/PENN STATE, STATE COLLEGE, PA (Dr. S. McDaniel, Dr. D. McCammon, Dr. F. Symon)	3
CYBERLINK, Boulder, CO (Dr. P. McManamon)	1
APL/JOHNS HOPKINS UNIV (Dr. J. Apel)	1
WPL-NOAA (Wave Propagation Lab (Dr. S. Clifford))	1
NOAA (Dir. of NOAA Labs, (Dr. V. Derr))	1
JOHNS HOPKINS UNIV (Dept. of Oceanography (Prof. O. M. Phillips))	1
UNIV OF WISCONSIN (Dept. of Geophysics (Prof. C. S. Clay))	1
UNIV OF NEW MEXICO (Dept. of Elec. Eng . (Prof. D. Petersen))	1
PSI, Inc. (Dr. R. Mellen, J. Fitzgerald, Dr. J. Davis)	3
UNIV OF MIAMI/RSMAS (Dr. F. Tappert)	1
Dr. David Middleton, New York, NY	15
APL/UW (E. Thorsos, D. Jackson, S. McConnell)	3
ONT (T. Warfield, B. Palmer)	3
NADC (Code 3042 (T. Polaneczky))	1
UNIV OF ILLINOIS (V. Twersky)	1
FWG/Kiel, Germany (Prof. Dr.-Ing. G. Ziehm, Dr.-Ing. H. Herwig, Dipl.-Ing. B. Nuetzel)	3
UNIV OF KANSAS (Dr. R. T. Lawner, Dr. R. K. Moore)	2
SONALYSTS, Inc. (W. Pugliese)	1
UNIV OF WASHINGTON (Dept. of Elec. Eng. and App. Math (Prof. A. Ishimaru))	1
UNIV OF NEBRASKA (Dept. of Elec. Engr. (Prof. E. Bahar))	1
DARPA (C. Stewart)	1
NCSC (Dr. L. Satkowiak)	1
GEORGE MASON UNIV (Dr. E. Wegman)	1
BOLT, BERANEK & NEWMAN (Dr. P. Cable, J. Hanrahan, T. Kooij)	3